

Cosmic-ray Neutron Spectrometry and Dosimetry

Takashi Nakamura*

Tohoku University, Cyclotron and Radioisotope Center, Sendai, Japan

When primary cosmic rays consisting of galactic cosmic rays and solar particles come into the earth's atmosphere, secondary neutrons generated through nuclear reactions with atmospheric atoms reach the ground. Over the past 10 years, there has been increasing concern about the exposure of air crews to atmospheric cosmic radiation. At aviation altitudes, the neutron component of the secondary cosmic radiation contributes about half of the dose equivalent. Recently, an accumulation of the semiconductor device greatly increases and the soft-errors of SRAM and DRAM on the ground level caused by high-energy cosmic-ray neutrons become a serious problem in the world. Under these circumstances, cosmic-ray neutron spectrometry and dosimetry are presented here in the terrestrial and space environments where neutrons and protons coexist.

The neutron detection methods for use in this mixed field are described; 1) multi-moderator spectrometer (Bonner Ball), 2) organic liquid scintillation spectrometer, 3) dose-equivalent counter (rem counter) and 4) Phoswich-type detector. Using these detectors, neutron energy spectra and dose-equivalent rates have been measured on the ground at sea level and at mountain level, aboard an airplane and in space. The space experiments were done using a balloon, space shuttle and space station. The neutron spectrum on the ground has three major peaks, thermal energy peak, evaporation peak around 1 MeV and cascade peak around 100 MeV. While on the other hand, the neutron spectrum apart from the ground has no thermal neutron peak that comes from the albedo neutron effect backscattered from the terrestrial surface. The time-sequential experimental results in Japan, Europe and U.S.A. are described with the experimental procedures by paying attention to variation with latitude, altitude and solar activity.

KEYWORDS: *cosmic-ray neutrons, altitude, latitude, solar activity, sequential measurement, neutron detector*

I. Introduction

When primary cosmic rays consisting of galactic cosmic rays and solar particles come into the earth's atmosphere, they produce secondary cosmic rays through many cascade reactions with atmospheric atoms. Over the past 10 years, there has been increasing concern about the exposure of air crews to atmospheric cosmic radiation. At aviation altitudes, the neutron component of the secondary cosmic radiation contributes about half of the dose equivalent. At terrestrial altitudes, strongly penetrating particles such as muons and neutrons can reach sea level. At sea level, cosmic rays are about 90% ionizing radiation consisting mostly of muons with some electrons and also photons, and about 10% neutrons. The recent dramatic rise in the use of semiconductor devices has resulted in a corresponding increase in the soft-errors of SRAM and DRAM at ground level, caused by high-energy cosmic-ray neutrons. This is a serious problem world wide.

Under these circumstances, many neutron measurements aboard the airplane and on the ground at different elevations have been done in Europe and North America,¹⁻³⁾ mainly at high geomagnetic latitudes, however, only one measurement has been done aboard an airplane over Japan at low geomagnetic latitude on February 27, 1985.⁴⁾ Here in this paper, cosmic-ray neutron spectrometry and dosimetry are presented in the terrestrial and space environments where neutrons and protons coexist.

The characteristic feature is that the depth dependence of total neutron flux has a maximum at an altitude of 15 – 20 km (55 – 125 g/cm² depth) above sea level. This maximum occurs at all latitudes and arises as a result of two processes: secondary particle cascade development and neutron leakage/attenuation through the atmosphere, which is referred to as the cascade maximum. At depths in the atmosphere exceeding about 150 g/cm², the total neutron flux shows an exponential decrease with depth characterized by the effective attenuation length.⁵⁾ In the vicinity of the air/ground interface, the equilibrium of neutron fields is disturbed due to the albedo neutron effect backscattered from the terrestrial surface, which generates an increase of thermal neutron flux.

II. Neutron Detection Method

Various conventional and newly-developed detectors have been used for neutron measurements in the terrestrial field and aboard airplanes. In this paper, two types of spectrometers, the multi-moderator spectrometer, so-called Bonner ball, and the organic liquid scintillation spectrometer are described. One type of dose meter, the dose equivalent counter, so-called rem counter, is also described along with the Phoswich-type detector for use in a mixed radiation field.

1. Multi-Moderator Spectrometer (Bonner Ball)

The multi-moderator spectrometer, Bonner ball, has been widely used for neutron spectrometry in nuclear facilities and in the natural environment due to its simplicity and the usability over a wide range of neutron energies spanning from thermal to MeV. However, the energy resolution is poor

*Corresponding Author, Tel/Fax: +81-422-54-7899 E-mail: nakamura@cyric.tohoku.ac.jp

and an initial guess spectrum is required. Uwamino and Nakamura developed the Bonner ball more than 20 years ago.⁶⁾ It has a high neutron sensitivity and uses only five polyethylene moderators. This type of Bonner ball is now widely used in Japan as a standard detector. The Bonner ball is composed of spherical ^3He proportional counters (5.07 cm in diameter, filled with 5 atm ^3He gas manufactured by LND Inc.) covered with polyethylene moderators. Neutrons having energies degraded in the polyethylene through the $\text{H}(n,n)p$ elastic scattering reaction can be detected with a central ^3He counter through the $^3\text{He}(n,p)$ reaction. The thicknesses and the diameters of the polyethylene moderators are 0 cm (bare), 8.0 cm (1.5 cm thick), 11 cm (3.0 cm thick), 15 cm (5.0 cm thick), and 23 cm (9.0 cm thick), respectively. The detector response functions required to convert measured count rates to a neutron energy spectrum are given by Uwamino et al.⁶⁾ and by Nunomiya⁷⁾ using the MCNPX (version 2.1.5) code⁸⁾ in the energy range from thermal to 1 GeV, as shown in **Fig. 1**.

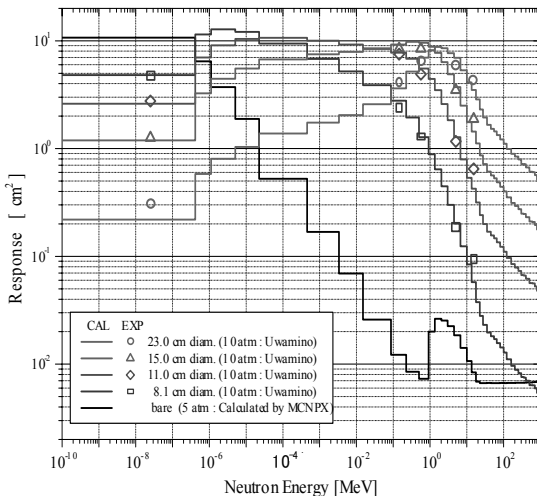


Fig. 1 Measured and calculated response functions of multi-moderator spectrometer⁸⁾

Goldhagen et al. developed a Bonner ball designed specifically for cosmic-ray neutron measurements.³⁾ Its 14 detectors are spherical 5.08 cm-diameter ^3He -filled proportional counters, with one unshielded, one surrounded with a layer of cadmium, and the rest surrounded with high-density polyethylene spheres having diameters ranging from 6.7 to 38 cm. In order to create a rising response with increasing energy, beyond 20 MeV, one detector has a 25-kg lead shell embedded in its moderator, and another has an 18-kg steel shell.

2. Organic Liquid Scintillation Spectrometer

NE213 (or BC501A) organic liquid scintillators coupled with photo-multipliers are widely used for high energy neutron spectrometry in target and shielding experiments due to the high quality of neutron and photon discrimination, along with the excellent energy resolution. In general, neutron spectra can be obtained from these detectors using an unfolding technique. Neutron and photons incident on

the organic scintillator mainly produce protons through the $\text{H}(n,n)p$ reaction and electrons through Compton scattering, respectively. The light output pulses from neutron-induced protons are slower than those from photon-induced electrons, which enables the pulse-shape discrimination between neutron and proton events. For higher energy neutron measurements, a large-size NE213 detector, 12.7-cm diam. by 12.7-cm long, coupled with a photomultiplier (Hamamatsu R4144) has been used by our group. With regard to the response functions of the 12.7-cm diam. by 12.7-cm long NE213 detector for neutrons above 20 MeV, Nakao et al.⁹⁾ measured those functions for energies up to 206 MeV using the $^7\text{Li}(p,n)$ quasi-monoenergetic and white neutron sources at the ring cyclotron facility (RRC) of the Institute of Physical and Chemical Research (RIKEN), Japan. Sasaki et al.¹⁰⁾ extended those functions up to 800 MeV using the white neutron source from thick carbon target bombarded by 400 MeV/nucleon carbon and 800 MeV/nucleon silicon ions at the Heavy Ion Medical Accelerator facility (HIMAC) of National Institute of Radiological Sciences (NIRS), Japan.

3. Dose-Equivalent Counter (Rem Counter)

Two types of high sensitivity rem counters were fabricated by Nakamura et al. using large volume and high pressure ^3He spherical proportional counters, one filled with 10 atm ^3He and having a 5.08 cm (2 in.) diameter, the other one filled with 5 atm ^3He and having a 12.7 cm (5 in.) diameter.¹¹⁾ The responses of these two rem counters to neutrons of energies from thermal to 15 MeV are shown in **Fig. 2** along with comparisons to the response of the first Anderson-Braun (A-B) type rem counter, the widely-used Studsvik 2202D, and the formerly-used fluence-to-dose conversion factor given by ICRP-21.¹²⁾ Our 2-in.-diam. and 5-in.-diam. ^3He rem counters have about 10 and 70 times higher sensitivities than the Studsvik 2202D rem counter, respectively. At present, they still have highest sensitivities among the commercially available rem counters in the world.

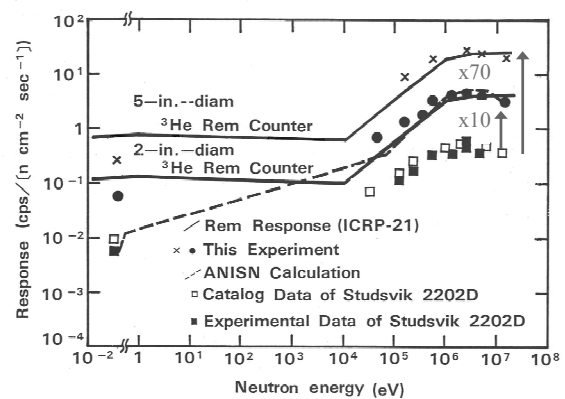


Fig. 2 Measured response functions of two high-sensitivity rem counters using 2 and 5-inch-diam. ^3He detectors, and the Studsvik 2202D rem counter, with the fluence-to-dose conversion factor by ICRP Publication 21 and the response calculated by ANISN¹¹⁾

Because all conventional A-B type rem counters underestimate the neutron dose above 20 MeV due to low sensitivity, Birattari et al. developed a new-type rem counter, called LINUS, that extended the measurable neutron energy range above 20 MeV.¹³⁾ They inserted a 1-cm thick layer of lead between the inner and outer polyethylene moderator layers, just outside the borated rubber. The central part comprises a spherical ^3He proportional counter of 3.2 cm active diameter filled with 304 kPa ^3He and 101 kPa Kr. The effect of the additional lead layer is to detect neutrons with energy greater than about 10 MeV via evaporation neutrons produced in inelastic scattering and $\text{Pb}(n,2n)$ reactions.

4. Phoswich-Type Detector

In the phoswich detector developed by Takada et al.,¹⁴⁾ the two scintillators of NE115 and NE213 are optically coupled to a single photomultiplier tube (Hamamatsu H1949). The liquid scintillator is surrounded by a thin slow plastic scintillator (NE115, 5 mm thick) with a low sensitivity to neutral particles. The inner detector is a liquid organic scintillator (NE213, 58.5 mm diam and 58 mm length, which corresponds to the range of 70 MeV proton) contained in a glass cell and has much greater sensitivity to neutrons. Charged particles are detected by both scintillators. The light output pulse in the NE115 from charged particles has a long characteristic time constant of about 225 ns, whereas the light output pulse in the NE213 from recoil protons produced by energetic neutrons has a time constant of about 30 ns. The time constant from Compton electrons produced by gamma rays is about 3.7 ns. These differences in the light-decay time constant make it possible to separate pulses of the three different particle species.

A new radiation dose monitor, designated as DARWIN (Dose monitoring system Applicable to various Radiations with Wide energy raNges), has been developed by Sato et al.¹⁵⁾ DARWIN is composed of a phoswich-type scintillation detector that consists of a liquid organic scintillator BC501A coupled with $\text{ZnS}(\text{Ag})$ scintillation sheets doped with ^6Li . Scintillations from the detector induced by thermal and fast neutrons, photons and muons were discriminated by analyzing their waveforms. Dose from neutrons below 1 keV is evaluated from the number of scintillations from the $\text{ZnS}(\text{Ag})$ sheets, while those from neutrons above 1 MeV, as well as photons and muons, are estimated from the light output of scintillations from BC501A.

III. Experimental Procedure

1. Neutron Measurements on the Ground at Several Locations

The sequential measurements of neutron energy spectrum and dose equivalent have been done at four places, two in Japan,^{16, 17)} one in U.S.A.¹⁸⁾ and in Germany,¹⁹⁾ in order to investigate the long-term changes of cosmic-ray neutron flux and dose rate on the ground. The former two measurements in Japan have been done over two years, while the latter two measurements were done in less than one year. The long-

term sequential measurements using three types of neutron detectors, Bonner ball, high-sensitivity rem counter and NE213 organic liquid scintillator were done in an experimental cabin set up on the ground at the Kawauchi campus of Tohoku University in Sendai, Japan from April 2001 to March 2003.¹⁶⁾ The measuring position is situated at latitude $38^\circ 15'$ north and longitude $140^\circ 52'$ east and an altitude of about 70 m. The geomagnetic latitude in Sendai is about 29°N , and the cut-off rigidity is 10.43 GV. Following this study, a group in the Japan Chemical Analysis Center measured cosmic-ray neutrons with the same type of the Bonner ball and the 5-in.-diam. ^3He rem counter (model NDN4NA11 fabricated by Fuji Electric Systems Co. Ltd.), as used in Sendai. The measurements have been taken sequentially from March 2002 up to the present at a site in Chiba, Japan.¹⁷⁾ The geomagnetic latitude in Chiba is about 26.6°N .

Kowatari et al. investigated the altitude variation of the cosmic-ray neutron component in low geomagnetic latitude.²⁰⁾ They measured the neutron energy spectrum at various altitudes in the Mt. Fuji area (26°N geomagnetic latitude, altitude: 40 m – 2400 m) using the Bonner ball described before. In parallel with the neutron energy spectrum measurement, the measurement of the neutron ambient dose equivalent was also done by using a commercially available neutron rem counter in the same area (altitude: 40 m – 3776 m).

2. Neutron Measurements Aboard an Airplane and in Space

Nakamura et al.⁴⁾ measured the altitude variation of the cosmic-ray neutron energy spectrum and dose equivalent aboard an airplane by using the Bonner ball and the 5-in.-diam ^3He rem counter. The data were obtained on a flight February 27, 1985 (solar minimum period) of a DC-8 aircraft of Japan Air Lines chartered by the Institute of Physical and Chemical Research (RIKEN). The flight from the Narita Airport, proceeded west, keeping the geomagnetic latitude at approximately 24°N , and returned to the Narita Airport. During a total flight time of 2.2 h, the aircraft was flown for 60 min at an altitude of 4880 m, and for a period of 20 min at 11280 m for the cosmic-ray neutron spectral measurements. The AIR ER-2 flights were scheduled for June 1997, a time of maximum galactic cosmic radiation (solar minimum), and were designed to cover as wide a range of latitude and altitude as possible within the operational capabilities of the ER-2.³⁾ There were five measurement flights. All flights originated at the NASA Ames Research Center (37.4°N , 122°W) in California and started with a northward climb. The East flight provided a long period of nearly constant radiation level by flying at constant geomagnetic cutoff. The rest of the flights measured the effects of latitude and of altitude at low geomagnetic cutoffs. The East and the two North flights included an altitude dip while flying magnetic west at constant geomagnetic cutoff, allowing measurements at altitudes from 21.3 km (70,000 ft) down to 16 km (52,500 ft). Overall, the flights covered latitudes from 18° to 60°N , corresponding to

geomagnetic vertical cutoff rigidities from 12 GV to 0.4 GV, and atmospheric depths from 50 to 110 g/cm².

Nagaoka *et al.* measured the altitude variation of neutron ambient dose equivalent rate using a balloon.²¹⁾ A balloon was at sea level by JAXA on August 25, 2004 from Sanriku Balloon Center, Iwate, Japan, and rose to an altitude of 25 km. The geomagnetic latitude at the Sanriku Balloon Center is 30.2°N and the cutoff rigidity is 9.2 GV. A portable survey-meter type (Type NSN 21011, Fuji Electric Systems Co.) neutron rem counter and an identical counter covered with additional polyethylene moderator (2 cm thickness) were installed into a pressure vessel of 2 mm thick aluminium. The balloon was collected on the next day after 1 day of flight. The measurement was taken during a period of average solar activity.

The same type of Bonner ball was fabricated by the National Space Development Agency (NASDA, now JAXA: Japan Aerospace Exploration Agency) for use in space. The Bonner ball was mounted in the SPACEHAB module in the space shuttle cargo bay. The neutron energy spectrum in the shuttle was measured from January 24 to 28, 1998, in S/MM-08 (STS-89).²²⁾ Measured data and orbital information were transferred through downlink to the NASA Johnson Space Center Mission Control Center and transmitted for analysis to Tsukuba Space Center, NASDA. This Bonner ball was also used in the US module of ISS (International Space Station, altitude 400 km) by NASA to measure neutron dose from March 23 to July 6, 2001.²³⁾

IV. Results and Discussions

1. Neutron energy Spectrum

Fig. 3 exemplifies the neutron energy spectra measured by Nakamura *et al.* at Tohoku University, Sendai on three different days, May 12, July 12, September 6 in 2002.¹⁶⁾ Each data set was obtained for 12 hours using the Bonner ball. These spectra were obtained by unfolding with the SAND-2 code²⁴⁾ and the initial guess spectrum given by Goldhagen *et al.*³⁾ Three peak components can be seen in **Fig. 3**. The first highest peak is a cascade peak component, which appears around 100 MeV.

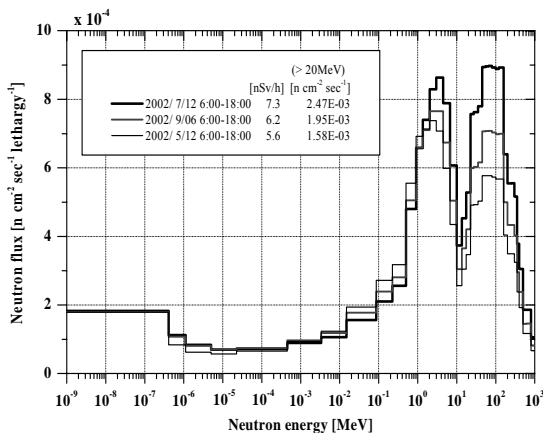


Fig. 3 Comparison of neutron energy spectra on three different days, July 12 (high flux), September 6 (medium flux) and May 12 (low flux) in 2002, measured by the Bonner ball¹⁶⁾

This component fluctuates about 30% from day to day and has a clear tendency to increase on the day of relatively higher solar activity which in turn corresponds to a higher neutron flux. The second middle peak is an evaporation peak component, which appears around a few MeV. The third lowest peak is a thermal neutron peak component, which appears below about 1 eV. The peak values of the second and, in particular, the third components keep almost constant values of about 7.5×10^{-4} (n cm⁻² s⁻¹ lethargy⁻¹) and about 1.8×10^{-4} (n cm⁻² s⁻¹ lethargy⁻¹), respectively.

Fig. 4 gives the cosmic-ray neutron energy spectra in lethargy unit at different atmospheric depths (altitudes) obtained by Goldhagen *et al.*³⁾ in June, 1997 (solar minimum period) and by Nakamura *et al.*⁴⁾ on February 27, 1985 (solar minimum period), together with the average value at sea level obtained in the study conducted on September 6, 2002 (solar maximum period) by Nakamura *et al.*¹⁶⁾

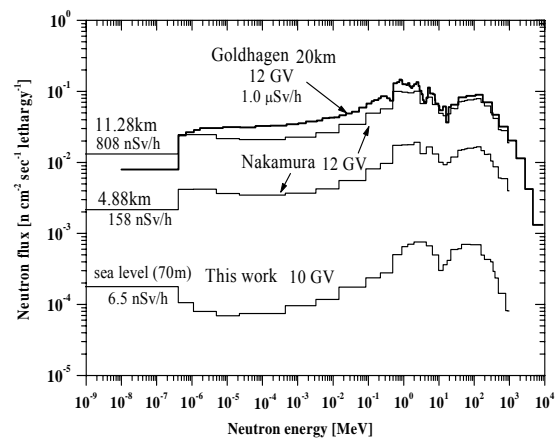


Fig. 4 Cosmic-ray neutron energy spectra in units of lethargy at different atmospheric depths (altitudes) by Goldhagen *et al.*³⁾ in June, 1997 and Nakamura *et al.*⁴⁾ on February 27, 1985, with the value at sea level on September 6, 2002 by Nakamura *et al.*¹⁶⁾

The three spectra at high altitudes (20 km, 11.28 km and 4.88 km) having a similar cutoff rigidity of 12 GV show similar spectral shapes, although Goldhagen's spectrum is a little bit higher in the energy region below the evaporation peak around 1 MeV than Nakamura's spectrum. They are also similar in the MeV region to the spectrum measured at sea level at a cutoff rigidity of 10 GV, with two prominent peaks around 1 MeV and 100 MeV. However, in the energy region lower than 1 MeV, the spectrum becomes softer with increasing atmospheric depth, and the thermal energy peak can be found at sea level, which indicates neutron thermalization through the atmosphere and backscattering from the earth, as described before. In spite of the large time intervals between these neutron measurements, the energy spectra have not changed very much. This spectral equilibrium might be due to poor energy resolution and the strong dependence of the initial-spectrum guess of the Bonner ball, especially in high-energy region.

Fig. 5 shows the neutron energy spectra observed at three geomagnetic regions: the Polar region, the SAA (South

Atlantic Anomaly) region, and the Equatorial region, from January 24 to 28, 1998 on S/MM-08 (STS-89) in the SPACEHUB module in the space shuttle.²²⁾ The spectra were determined by unfolding with the SAND-2 code and the 1/E initial guess spectrum. The three spectral shapes are very close to each, but the absolute values are different. The total neutron fluxes were 7.64 to 112.95 $\text{cm}^{-2} \text{s}^{-1}$ for the SAA region and 0.35 to 7.97 $\text{cm}^{-2} \text{s}^{-1}$ for the other two regions. The average ambient dose equivalent rates were 45.8 $\mu\text{Sv/h}$ for the SAA region and 3.01 $\mu\text{Sv/h}$ for the other regions.

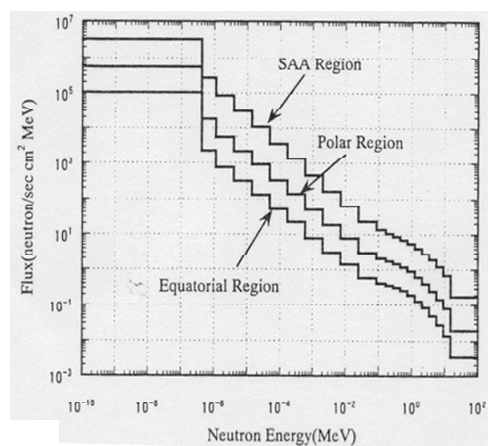


Fig. 5 Neutron energy spectra in the space shuttle STS-89 measured with a Bonner ball²²⁾

2. Time-sequential Results of Neutron Ambient Dose Equivalent Rates

Neutron ambient dose equivalent rates obtained by using a rem counter remains almost constant at about 4.0 nSv/h,

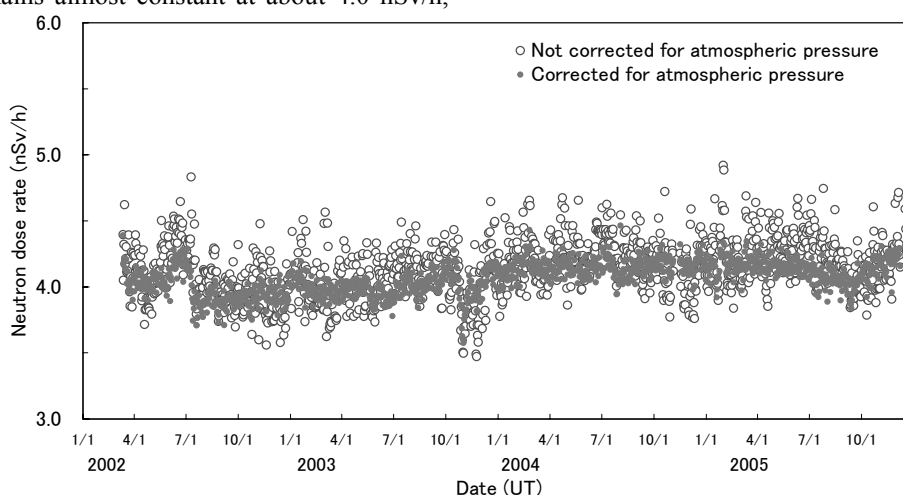


Fig. 6 Time-sequential data of neutron ambient dose equivalent rates measured by a rem counter from March, 2002 to December, 2005 in Chiba, Japan¹⁷⁾

3. Variation with Latitude, Altitude and Solar Activity

Fig. 7 gives the altitude variation of neutron ambient dose equivalent rates (nSv/h), as measured by Nakamura et al.⁴⁾, Goldhagen et al.³⁾ (both in an airplane), by Kowatari et al.²⁰⁾, Matsumoto et al.²⁶⁾ (both on the ground at the Mt. Fuji

with a variation of about 5% over the entire time period between April 2001 and March 2003 at Tohoku University, Sendai by Nakamura et al.¹⁶⁾ However, there are some remarkable variations. The neutron ambient dose steeply decreased about 30%, and this phenomenon remained for a few days, when it snowed on the Kawauchi campus, and about 20 cm of snow piled up on the cabin. This steep decrease in ambient dose equivalent was caused by neutron attenuation through the hydrogen in the snow. Especially on April 16, large solar flares were observed by the ACE satellite and the neutron dose rates decreased by about 10%. This phenomenon is called the Forbush decrease. The dose rates estimated by multiplying the Bonner ball spectrum with the fluence-to-ambient dose equivalent conversion factor given by ICRP 74²⁵⁾ are also given for comparison. The average value of dose rates given by the Bonner ball is 6.5 nSv/h and is about 60% higher than 4.0 nSv/h given by the rem counter, because the rem counter has very low sensitivity to neutrons of energy above 20 MeV.

The following sequential measurements using a similar rem counter have been done at the Japan Chemical Analysis Center (JCAC), Chiba from March 2002 up to the present.¹⁷⁾

Fig. 6 shows the neutron ambient dose equivalent rates averaged over each day in units of nSv/h measured with a 5-in.-diam ³He rem counter. The dose rates are normalized to 1 atm (1013 hPa) to correct for differences in atmospheric pressure. The normalized dose rates indicate a big Forbush decrease from the end of October to the beginning of November, 2003, and a small Forbush decrease at the beginning of September, 2005, which reflect the big solar flares from October 28 to November 4, 2003, and from September 7 to 9, 2005.

area), along with the result on the ground by Nakamura et al.¹⁶⁾ The graph shows that the cosmic-ray neutron variation with altitude exhibits an exponential attenuation, $\exp(-D/\lambda)$, as a function of atmospheric depth, D , up to about 7 km height above the ground. It approaches a saturated value near 20 km height, which is near the cascade maximum. From the

exponential attenuation curves, the attenuation lengths for neutron ambient dose equivalent determined by Bonner ball measurements are 144 g/cm^2 . A smaller value of 135 g/cm^2 is determined by rem counter measurements, since the rem counter is mainly sensitive to neutrons below 20 MeV. The attenuation lengths are determined to be 155 g/cm^2 for total neutron flux and 165 g/cm^2 for neutron flux above 20 MeV. These values are quite similar to the values between 140 and 165 g/cm^2 listed by Ziegler et al.⁵⁾

The ambient dose equivalent rates measured with two types of rem counters launched in a balloon up to 25 km above the sea level in Japan (about 10 GV) are shown in **Fig. 8**.²¹⁾ The results are compared with other experimental and calculated results at 0.8 GV and 12 GV. The UNSCEAR results calculated at high latitude²⁷⁾ and the Goldhagen results at 0.8GV³⁾ are much higher than the results at low latitude with 10 and 12 GV cutoffs.

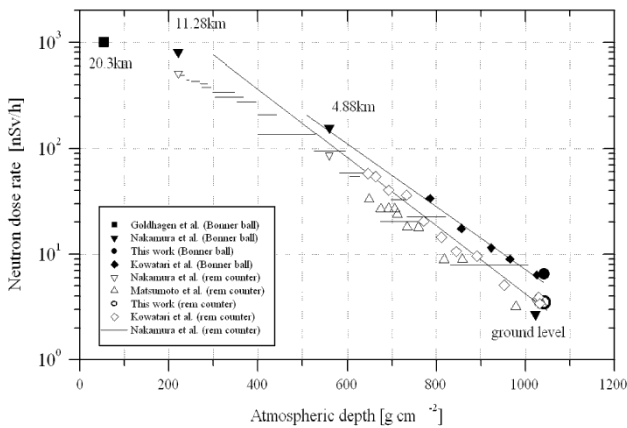


Fig. 7 Altitude variation of neutron ambient dose equivalent rates (nSv/h) measured by Nakamura et al.⁴⁾, Goldhagen et al.³⁾ (both in an airplane), by Kowatari et al.²⁰⁾, Matsumoto et al.²⁶⁾ (both on the ground at the Mt. Fuji area), and by Nakamura et al.¹⁶⁾ at sea level.

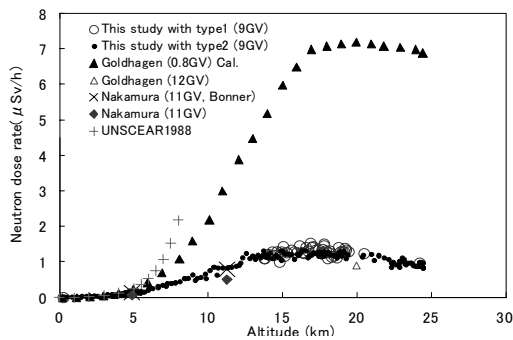


Fig. 8 Altitude variation of ambient neutron dose equivalent rates measured with two types of rem counters launched in the balloon up to 25 km above Japan on August 25, 2004,²¹⁾ with other results by Nakamura et al.⁴⁾, Goldhagen et al.³⁾ and the UNSCEAR results²⁷⁾.

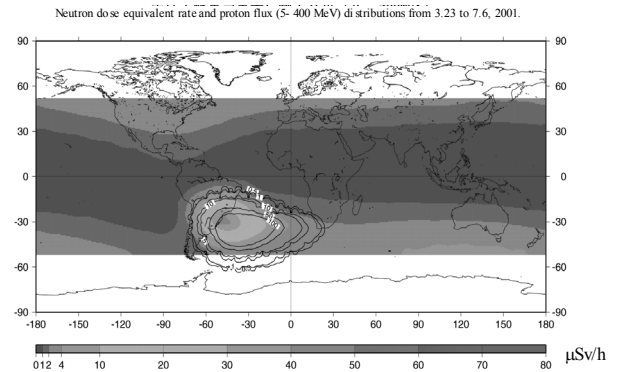


Fig. 9 World map of neutron ambient dose equivalent rates measured by the Bonner ball above about 400 km from March 23 to July 6, 2001, overlapped with proton flux distribution of energies from 5 to 400 MeV²³⁾

The variation of total neutron ambient dose equivalent rate as a function of geomagnetic latitude has also been measured by many researchers. **Fig. 9** gives the summarized results of ambient dose equivalent rate.¹⁷⁾ The neutron dose rate increases with the latitude from the equator to the pole which is a result of the geomagnetic effect.

Fig. 10 shows the neutron ambient dose equivalent rate distribution in $\mu\text{Sv/h}$ on a world map measured in the US module of the ISS about 400 km above the earth from March 23 to July 6, 2001.²³⁾ The neutron dose rate distribution is overlapped with the proton flux distribution for energies from 5 to 400 MeV. The neutron and proton flux distributions are well correlated with each other, giving high intensities at the SAA region. This indicates that neutrons are produced mainly from protons through nuclear reactions in the air. Solar activity also has an effect on neutron flux and dose rate on the ground. The inverse correlation between heliocentric potential and neutron intensity is clearly seen from 2002 towards 2005, which means that the shielding effect on primary cosmic radiation entering into the earth becomes stronger with increasing the solar activity.

V. Conclusion

The terrestrial neutron energy spectrum and ambient dose equivalent rate are reviewed here.

The shapes of neutron energy spectra on the ground for different geomagnetic altitudes and latitudes are similar and typically have three prominent broad peaks. There is a peak around 100 MeV caused by cascade neutron production, a peak around 1 MeV caused by evaporation process, and a peak in thermal energy region due to neutron thermalization through the atmosphere and backscattering from the earth. In the air aboard an airplane and in space, however, thermal neutron peaks can not be found in the spectra. The absolute values of the neutron flux and ambient dose equivalent are strongly dependent on the altitude and latitude.

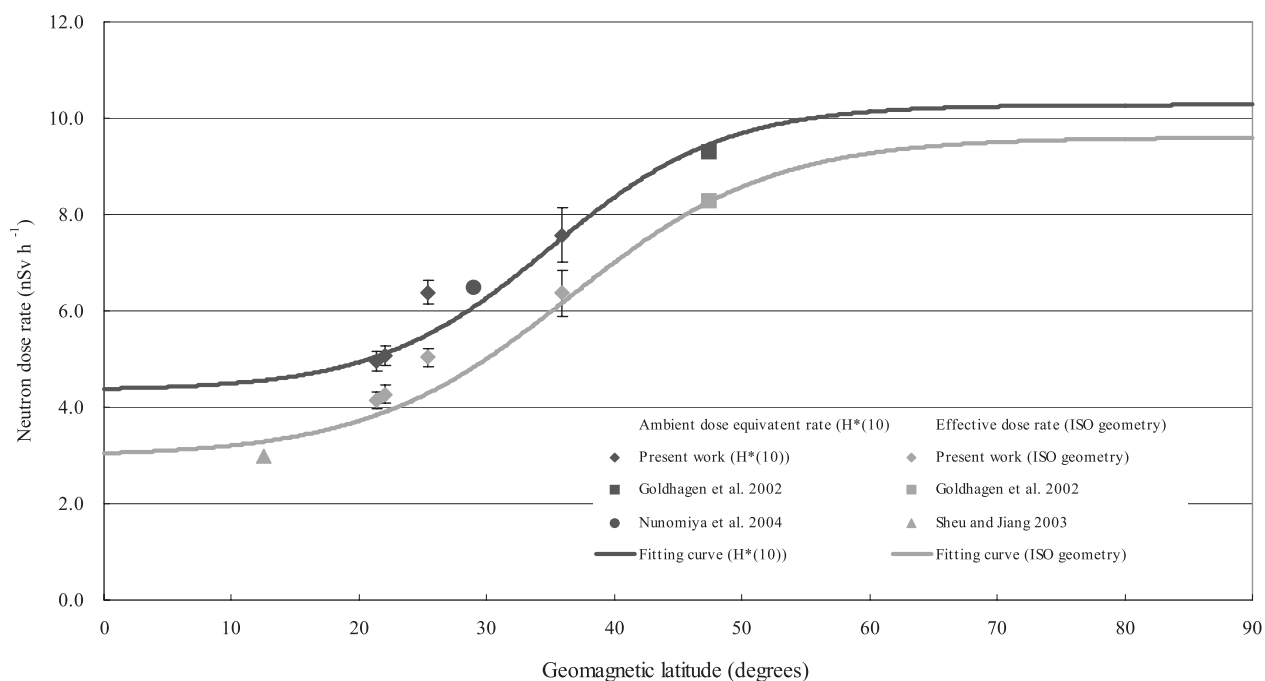


Fig. 10 Geomagnetic latitude variation of the cosmic-ray neutron ambient dose equivalent and effective dose rates¹⁷⁾, Present work by Kowatari et al.¹⁷⁾, Goldhagen et al.³⁾, Nunomiya et al.²⁸⁾ and Sheu and Jang²⁹⁾.

References

- 1) U.J. Schrewe, *Radiat. Protec. Dosim.*, **91**, 347 (2000).
- 2) B.J. Lewis, M.J. McCall, A.R. Green, et al., *Radiat. Protec. Dosim.*, **93**, 293 (2001).
- 3) P. Goldhagen, M. Reginatto, T. Kniss et al., *Nucl. Instr. and Meth.*, **A 476**, 42 (2002).
- 4) T. Nakamura, Y. Uwamino, T. Ohkubo, A. Hara, *Health Phys.*, **53**, 509 (1987).
- 5) J.F. Ziegler, *IBM J. Res. Develop.*, **40**, 19 (1996).
- 6) Y. Uwamino, T. Nakamura, A. Hara, *Nucl. Instr. Meth.*, **A 239**, 299 (1985).
- 7) T. Nunomiya, "Study on the deep penetration of neutrons produced by high-energy accelerator and cosmic ray", Doctor Thesis of Tohoku University, (2003), [in Japanese].
- 8) L. S. Waters, (Ed.), LA-CP-02-408, Los Alamos National Laboratory, Los Alamos, New Mexico (2002).
- 9) N. Nakao, T. Kurosawa, T. Nakamura, Y. Uwamino, *Nucl. Instr. and Meth.*, **A463**, 275 (2001).
- 10) M. Sasaki, N. Nakao, T. Nakamura, et al., *Nucl. Instrum. Methods*, **A 480**, 440 (2002).
- 11) T. Nakamura, A. Hara, T. Suzuki, *Nucl. Instrum. Methods*, **A241**, 554 (1985).
- 12) International Commission on Radiological Protection, ICRP Publication 60, *Ann. ICRP* 21 (1991).
- 13) C. Birattari, A. Esposito, A. Ferrari, et al., *Radiat. Protec. Dosim.*, **76**, 135 (1998).
- 14) M. Takada, S. Taniguchi, T. Nakamura, K. Fujitaka, *IEEE Trans. on Nucl. Sci.*, **45**, 888 (1998).
- 15) T. Sato, D. Satoh, A. Endo, Y. Yamaguchi, *J. Nucl. Sci. Technol.*, **42**, 768 (2005).
- 16) T. Nakamura, T. Nunomiya, S. Abe, et al., *J. Nucl. Sci. Technol.*, **42**, 843 (2005).
- 17) K. Nagaoka, Private communications, August 2006: M. Kowatari, Y. Ohta, S. Satoh, et al., *J. Nucl. Sci. Technol.*, **44**, 114 (2007)..
- 18) M.S. Gordon, P. Goldhagen, K.P. Rodbell, et al., *IEEE Trans. Nucl. Sci.*, **51**, 3427 (2004).
- 19) B. Wiegel, A.V. Alevra, M. Matzke, et al., *Nucl. Instr. and Meth.*, **A 476**, 52 (2002).
- 20) M. Kowatari, K. Nagaoka, S. Satoh, et al., *J. Nucl. Sci. Technol.*, **42**, 495 (2005).
- 21) K. Nagaoka, I. Hiraide, K. Sato, et al., *Proceedings of 10th Neutron Dosimetry Conference, Radiat. Protec. Dosim.*, in press.
- 22) H. Matsumoto, T. Goka, K. Koga, et al., *Radiat. Meas.*, **33**, 321 (2001).
- 23) H. Koshiishi, H. Matsumoto, K. Koga, T. Goka, *Annual Report 2002, Office of Research and Development, National Space Development Agency of Japan*, 2002, 151 (2002); *Radiat. Meas.*, in press.
- 24) W.N. McElroy, S. Berg, T. Crockett, R.G. Hawkins, *AFWL-TR-67-41, Air Force Weapons Laboratory* (1967).
- 25) International Commission on Radiological Protection, ICRP Publication 74, *Annals of the ICRP*, **26**, No.3-4, Elsevier Science, Oxford (1995).
- 26) M. Matsumoto, M. Furukawa, S. Tokonami, et al., *Radioisotopes*, **44**, 33 (1995), [in Japanese].
- 27) UNSCEAR 2000 Report to the General Assembly, with Scientific Annexes, Vol. I, United Nations Publication, New York (2000).
- 28) T. Nunomiya, S. Abe, N. Hirabayashi et al., *J. Nucl. Sci. Technol.*, *Suppl.* **4**, 466 (2000).
- 29) R.J. Sheu and S.H. Jiang, *Health Phys.*, **84**, 92 (2003).

Using Ionizing Radiation to Determine Trace Element Content in Living Human Subjects

David R CHETTLE*

McMaster University, Hamilton, Ontario, Canada

The use of ionizing radiation for medical procedures is very familiar, both for diagnosis, such as in radiography or nuclear medicine, or for therapy, such as external beam radiotherapy or brachytherapy. There are also many instances in which samples are analyzed for their elemental content in order to help diagnose or monitor a medical condition or environmental exposure. The use of ionizing radiation to measure the elemental content within the human body directly and non invasively has been developed and is used in a number of laboratories around the world. The *in vivo* analysis of trace and minor elements in this way has been termed Occupational Nuclear Medicine.

There are two general considerations that apply to Occupational Nuclear Medicine procedures. One is that the radiation dose to the subject must be carefully controlled and maintained within acceptable levels in all circumstances. The second is that both the probe that it used to excite a signal from the element of interest and the signal itself must be sufficiently penetrating for the signal to be detected with adequate sensitivity externally to the body. In practice, this means that photons or neutrons are used as the probe and that varieties of x-ray fluorescence and neutron activation are the techniques most commonly used.

For *in vivo* measurements, the use of x-ray fluorescence is confined to elements with relatively high atomic number, because the K shell x-rays are higher in energy and therefore more likely to escape from the body and the K shell fluorescence yield also increases with increasing atomic number. This presentation will examine measurements of both lead (Pb) and strontium (Sr) in bone. Pb is toxic, whereas Sr may confer strength on bone, although it is also damaging at high concentrations.

Cadmium (Cd) can be measured in liver and kidney by measuring γ -rays emitted promptly following neutron capture. Manganese (Mn) or aluminum (Al) can be measured in bone by counting induced radioactivity following neutron absorption. Although Mn is an essential element, it is the toxic effects of each of these elements, associated with chronic exposure and excessive accumulation in the body, that have motivated the development and application of these Occupational Nuclear Medicine techniques.

KEY WORDS: *x-ray fluorescence, neutron activation, in vivo elemental analysis, Pb, Sr, Cd, Mn, Al*

I. Introduction

Using ionising radiation to measure the elemental content of living human subjects is a somewhat unusual procedure and so it can appear untoward. However, it does in fact bear comparison with very well established techniques. The deliberate use of ionising radiation in medicine is so familiar as to be unremarkable. Radiation based techniques are routinely used for diagnosis. Within the broad category of radiography, there are numerous x-ray investigations and computerised tomography (CT) is very much a standard procedure. Within nuclear medicine, single photon emission computed tomography is very widely available and positron emission tomography is increasingly widely used as more medical cyclotrons are installed to provide the ^{18}F and other short lived isotopes that are usually employed in these investigations. As such techniques are developed they are subject to careful appraisal, as the benefit of the information they yield is balanced against the costs of the radiation dose administered to the subject and to the operators. Thus diagnostic techniques are required to be low dose, with an approximate upper end to the range of effective doses being

associated with whole body CT at around 10mSv. Much higher doses are commonly delivered in the course of radiation therapy, since the objective is to kill tumour cells while minimising damage to healthy tissue and maximising its chance for repair. Again, there is a variety of techniques routinely applied with external beam therapies involving gamma-rays and x-rays, including intensity modulated radiation therapy. In addition there are different forms of brachytherapy in which sources are introduced into the body. The point here is that the deliberate administration of radiation to human subjects for medical purposes is not at all unusual, rather it is a routine part of clinical practice. The analogy to be drawn here is between medical diagnostic procedures and using radiation to analyse elemental content *in vivo*.

Similarly, it is well established that there are many circumstances for which analysis of the elemental content of body tissues confers diagnostic value. This can be the analysis of an essential element such as calcium, for which there are well established normal ranges for the concentration in blood. Alternatively, it can be the analysis of an element such as lead, for which no essential function has been identified in the human body; so it is analysed to determine whether its concentration exceeds accepted

*Corresponding Author, Tel. +1-905-525-9140, Fax. +1-905-522-7776, E-Mail: chettle@mcmaster.ca

guideline values. These analyses are commonly performed on samples collected from a person's body, usually in blood or urine. Of course, such samples can be analysed for the presence of many other parameters beyond simple elemental content. The value of an element in blood indicates the level circulating in the body and thus gives information pertaining to a period of time of the order of weeks or less. Elemental content of urine provides information about an excretion pathway. Again this usually is most indicative of a relatively short time period. Other samples, such as hair or nail clippings can readily be collected, but it has proven difficult to relate analysis of these samples quantitatively to the metabolism of the element in the body. To do this, the information that most helpfully complements that, for example, from blood is the concentration of the element in a storage organ. A sample can be taken from bone, liver, kidney or another organ by means of a biopsy and this is again a standard medical procedure. However, biopsy is painful to the subject; it is not totally without risk and for these reasons it is not used in collecting information from large groups of subjects and, in particular, it is not normally used in studying healthy subjects.

It is in this context that a technique which can analyse the elemental content of a storage organ non invasively can be particularly valuable. This approach was applied to the measurement of calcium¹⁾, but that technique was superseded by dual energy x-ray absorptiometry, which provided fully adequate information on bone mineral status at a significantly lower dose and at lower cost of instrumentation than the neutron activation method that had been developed to measure calcium directly²⁾. Similarly, this approach can be used to measure total body nitrogen and hence infer total protein content and this neutron activation technique remains a method of choice in studies of the major components of body composition³⁾. However, this paper will address the challenges and successes encountered in measuring trace and toxic elements *in vivo* in living human subjects. Frequently the highest exposures to these elements, such as lead (Pb) and cadmium (Cd), occurs in the industrial setting, involving occupationally exposed workers. As there are analogies with other medical diagnostic procedures, such as nuclear medicine, the term "Occupational Nuclear Medicine" has been coined to describe such *in vivo* trace element analysis.

II. General Considerations

As with other radiation based medical diagnostic procedures, it is of primary concern to limit dose as far as reasonably possible and to ensure that it is delivered in a controlled manner and is monitored. Some of these procedures use neutron irradiations, so appropriate radiation weighting factors must be used⁴⁾. If the specific neutron energy spectrum is not known, it would be usual to assume a radiation weighting factor of 20, in order to err on the side of safety. Also, many of the measurements are of specific organs or parts of the body; so, tissue weighting factors need to be employed. Sometimes only a small proportion of a

tissue to which a weighting factor is attributed is irradiated. For example, small proportion of skin and of bone surface is irradiated in x-ray fluorescence measurements in bone. In this case a further factor, for example area of skin irradiated divided by total skin area, can be applied⁵⁾. It is also important to ensure that maximum local doses, often to skin, are kept within acceptable bounds. Such a skin dose should not exceed 150mSv. Tissue weighting factors are an internationally accepted guide, but it can also be helpful to assess the total energy absorption in the body⁶⁾, as this provides an alternative, albeit informal way of putting a partial body irradiation into context. Another helpful way of putting these diagnostic irradiations in context is to make the comparison with annual natural background radiation dose. Although this varies geographically, a figure of 3mSv per year is often cited. All these Occupational Nuclear Medicine procedures are subject to review by a Research Ethics Board, technique by technique and commonly on a study by study basis. As they are considered research procedures, informed consent is required from participants.

An essential and highly practical constraint is provided by the fact that the human body is an extended medium, even when the measurement is of a relatively small part of the body. In order to make a measurement of an element, several related criteria must be satisfied. A probe that is incident on the body must be capable of reaching the point in the body which is to be interrogated. This might be the kidney or liver, or it could be bone or even skin. The probe must be sufficiently penetrating, that is it must have a sufficiently long mean free path in tissue to reach the organ of interest. Secondly, the probe must interact with the element of interest and that interaction must produce an emission that is characteristic of the element. Thirdly, the characteristic emission from the reaction must itself have a sufficient mean free path to escape from the body. Lastly, the characteristic emission, having escaped, must be detected. In practice, photons (gamma-rays or x-rays) or neutrons nearly always provide the incident probe. There is a range of possible interactions, but the two most commonly used are the photoelectric effect (for incident photons) and neutron absorption. The large majority of these Occupational Nuclear Medicine Techniques therefore rely on x-ray fluorescence or neutron activation.

III. X-Ray Fluorescence

This area has been specifically reviewed by Börjesson and Mattsson recently^{7,8)}. Bone lead measured by x-ray fluorescence is the mostly widely used of these Occupational Nuclear Medicine techniques and it will be described in more detail below. Measurement systems for quite a wide range of elements have been at least attempted and many have been taken to full pilot study stage. For x-ray fluorescence, there is a clear advantage for measuring high atomic number elements, because the fluorescence yield increases with atomic number and the energy of the characteristic x-rays increases approximately as the square of atomic number, so the x-rays from high atomic number

elements are produced with higher probability and are more likely to escape from the body than those of low atomic number elements. The range of elements measured extends from iron ($z=26$)⁹ to uranium ($z=92$)¹⁰. Other elements measured include arsenic¹¹, silver¹², cadmium¹³, platinum¹⁴, gold¹⁵ and mercury¹⁶. The other element that will be considered here under the heading of x-ray fluorescence is strontium and the primary impetus for making such measurements is not its toxicity, but its beneficial effects in reducing the risk of fracture associated with osteoporosis.

1. Bone Pb

Three different x-ray fluorescence methods have been explored for *in vivo* measurement of lead (Pb) in bone. The first used gamma-rays (122keV, 136keV) from a ⁵⁷Co source to excite the Pb K x-rays¹⁷. Following this, an L x-ray system and the ¹⁰⁹Cd excited K x-ray system were developed at about the same time. The L x-ray system used either radioisotope sources or later the partly plane polarised output of an x-ray set with a silver target to excite the Pb L x-rays^{18,19}. At present, it is the ¹⁰⁹Cd system^{20,21} that is used in all but one of the laboratories around the world that conducts *in vivo* bone Pb measurements.

The energy of the gamma-rays emitted by ¹⁰⁹Cd (from the first excited state of ¹⁰⁹Ag) is 88.035keV. This is just greater in energy than the K shell absorption edge for Pb, at 88.005keV. This means that the photoelectric cross section is at a maximum for the Pb K shell, so the production of Pb characteristic K x-rays is as large as it could be. It also gives rise to a robust normalisation procedure, which makes this system particularly suitable for *in field* use.

The normalisation relies on taking the ratio of the K x-rays to the elastically scattered 88keV gamma-rays. For the normalisation to be effective, four criteria should be satisfied. (1) It should be the same incident fluence that produces both the x-rays and the elastically scattered gamma rays. Since the incident gamma-ray is so close in energy to the Pb K shell absorption edge, it is the uncollided incident gamma-rays that give rise to both x-rays and the elastic scatter feature. So the first criterion is satisfied. (2) The distribution of the sites of production of both the x-rays (from Pb) and elastically scattered gamma-rays should be the same. Since elastic scattering is very strongly dependent on atomic number, it comes almost exclusively from calcium and phosphorus in bone, rather than soft tissue. Also, Pb is distributed approximately uniformly in bone on the 5-10mm distance scale that relates to the mean free path of the incident gamma-rays and the emitted x-rays. In addition, Pb is concentrated in bone, so the emitted x-rays come from bone, rather than soft tissue. So the second criterion is to a large extent fulfilled. (3) The angular distribution of the two signals should be the same. X-ray emission is isotropic. Elastic scatter is very strongly forward peaked. However, the measurement geometry required for this ¹⁰⁹Cd excited x-ray fluorescence is as close to backscatter, that is 180°, as possible. This is to ensure as great a separation as possible in

energy between the Pb K x-rays and the Compton scattered incident gamma-rays. Although elastic scattering is strongly forward peaked, the cross section for this phenomenon is relatively invariant at this energy and in this medium (bone) between 120° and 180°. Since this range of angles encompasses those sampled in the measurement process, this third criterion is satisfied in the restricted geometry used in these measurements. (4) The two signals should be attenuated to the same extent and detected with the same efficiency. Neither aspect of this criterion is perfectly fulfilled, since the x-rays are slightly more attenuated in escaping from the bone and through overlying soft tissue. However, it is the x-rays that are detected with slightly greater efficiency in the hyperpure germanium detector. So these two deviations from identical behaviour are both small and they also tend to cancel each other out. So this fourth criterion is very largely satisfied. In establishing this technique, Somervaille²² carried out extensive experimental verification of the normalisation and she showed that this ratio of x-ray to elastic scatter is unaffected by source to sample distance, by thickness of overlying tissue, or by extreme variations in the radial distribution of Pb within a sample. It is also invariant, less remarkably, with duration of measurement and source activity.

So a bone Pb measurement system comprises a ¹⁰⁹Cd source, most typically of activity 1GBq. (The branching ratio for the emission of the 88keV gamma rays is low at 3.6%. Silver K x-rays are emitted with nearly 30 times the intensity of the 88keV gamma-rays and are attenuated through a copper filter of thickness 0.5 - 0.7mm.) The source is mounted in a heavy metal (tungsten alloy) collimator coaxially with and in front of the detector. Most current systems use a single hyperpure germanium crystal of diameter 50mm and thickness 20mm²³. Recently, a new system employing a stronger (5 - 10 GBq) source and a detector array comprising four smaller crystals (diameter 16 or 25mm, thickness 10mm) has been found to produce lower detection limits^{24,25}. The sample (person) is placed in front of the source-detector assembly, so gamma-rays are emitted by the source, undergo photoelectric effect, Compton scatter or elastic scatter in the sample and those x-rays or scattered gamma-rays that are approximately back scattered can reach the detector. The pulse processing electronics employed should preferably be one of the digital spectroscopy systems, as these have been shown to allow higher event throughput, without loss of energy resolution than conventional nuclear spectroscopy electronics²⁶. Data acquisition is usually not a rate limiting step and is accomplished with a system installed in a personal computer. Detection limits with the newer four crystal systems are now less than 5 µgPb/g bone mineral.

Research studies in which bone Pb measurements have played a key part have advanced the understanding of long term Pb metabolism significantly. It was quickly demonstrated that bone Pb correlates with age in subjects not occupationally exposed, with years of work in occupationally exposed people and only more weakly with current blood Pb in those same Pb workers. By far the

strongest of these correlations, however, is with a Cumulative Blood Lead Index (CBLI)²⁷. CBLI is the area under the curve when whole blood Pb is plotted against time. Typically it is estimated in Pb workers from records of blood Pb measurements made at least annually and sometimes as frequently as monthly. Estimates have to be made for exposure to Pb and the consequent blood Pb for times not covered by the work history. In many cases these estimates, usually of the time prior to the start of employment at a particular factory, form a relatively minor component of the overall CBLI. So uncertainties in these estimates do not greatly influence the calculated CBLI. It was expected that bone Pb would reflect cumulative exposure, so the strong correlation with CBLI was not a surprise. A second finding did have a greater impact on the way long term Pb exposure is viewed.

When bone Pb and blood Pb were examined in retired Pb workers, a strong correlation was observed between the two parameters^{28,29,30}. Furthermore, the retired Pb workers had higher blood Pb concentrations than referent groups with no occupational Pb exposure. Although the retired Pb workers had significantly lower blood Pb than those currently exposed to Pb. This is now interpreted as endogenous Pb exposure. That is, as Pb is slowly released from bone stores, it returns to blood and therefore maintains a blood Pb concentration that is raised above those of referent subject by an amount that depends on the amount of Pb stored in bone. This endogenous exposure is now brought into consideration when assessing the possible effects of past Pb exposures. It also receives particular attention in groups of people who are undergoing increased bone resorption, as this results in increased mobilisation of Pb from the bone stores. This most frequently affects women during pregnancy and lactation and at menopause. It can affect people of either sex when there is a disease or other event that can be expected to produce raised bone turnover. A third finding, which is still very much the focus of current research, became apparent when these endogenous relationships were examined in detail.

A simple regression relationship was found to be inadequate to describe the relationship between blood Pb and bone Pb in retired Pb workers. This implies some non linearity in the relationship³¹. This relationship is descriptive of the rate at which Pb is released from bone into blood. It appears that the higher the bone Pb concentration, the shallower the slope between blood Pb and bone Pb. This finding was confirmed when it became possible to make a second set of bone Pb measurements on a group of over 300 Pb workers³². This meant that a two point estimate could be made for each subject of the rate of release of Pb from bone, due allowance having been made for continuing exposure and for recirculation of Pb from existing bone stores within the body. It was found that subjects with higher bone Pb had significantly slower release rates of Pb from bone. When a different comparison was made within the overall group, it was found that older subjects released Pb from bone more slowly than did younger people³³. Within this overall study,

as within nearly all similar groups, bone Pb correlates strongly with age for two reasons. Firstly, older workers have worked more years and therefore had a longer time to accumulate Pb. Secondly, older subjects worked in the factory at an earlier time, when industrial hygiene was less stringent than it has been during the employment time of the younger workers. The study group was large enough that it was possible to select subgroups for one effect (eg age) while assessing the size of the other effect (bone Pb). Nevertheless, because the covariance between age and bone Pb is large, it still requires confirmation that these are two independent effects.

Although the work at McMaster has concentrated on studies of Pb metabolism, a very wide range of research has been conducted at other laboratories. It has now become accepted that research into long term health effects of Pb requires that bone Pb measurements be made³⁴, because there is no satisfactory alternative for assessing the cumulative Pb dose. So, with bone Pb as a benchmark, many studies of potential health effects of Pb have been carried out. These include the effects of normal aging³⁵, studies of hypertension amongst environmentally exposed subjects³⁶ and the impact of genetic variations on these effects^{37,38}. There have been extensive studies of maternal transfer of Pb to infants³⁹ and of the impact of Pb on child development⁴⁰. Although this last category would benefit from substantial further study with the more sensitive bone Pb instruments that have recently become available.

2. Strontium in Bone

Clinical trials have shown that strontium (Sr) administered to osteoporotic subjects can reduce the risk of bone fracture⁴¹. The underlying metabolism has not yet been elucidated, neither is it known why some subjects respond well to supplemental Sr, while others appear to derive no benefit. However, in excess, Sr can make bones brittle⁴². It is clear that a non invasive measurement of Sr as stored in bone can be expected to provide vital information both to provide a framework of understanding for Sr metabolism and to monitor the impact of treatment with Sr supplements.

An *in vivo* x-ray fluorescence measurement of Sr was first developed for use in animal studies⁴³. A system for human measurements was also developed in conjunction with the use of L x-rays to measure Pb in bone⁴⁴. Neither of these systems appears to be in current use, although the latter, which used the Ag x-rays from a ¹⁰⁹Cd source, is similar to one of the systems developed and used more recently. In fact a second radioisotope source, ¹²⁵I, has also been used and it is the ¹²⁵I which results in somewhat better system performance, although either source is definitely usable⁴⁵. In the present system at McMaster, a source of ¹²⁵I is mounted coaxially with and in front of a Si(Li) detector which has a 16mm diameter and 7mm thickness. The detector is coupled to digital spectroscopy electronics and a multichannel analyser. The mean free path of the Sr K x-rays (energies 14.1 and 16.0keV) is short. So, only superficial bone (<1.0mm) is sampled and the overlying tissue thickness has

to be measured (presently using ultrasound⁴⁶⁾) and a correction made for attenuation in this soft tissue. The minimum detectable level with this system is below $10\mu\text{gSr/g Ca}$, which appears to be comfortably below normal levels in the population in southern Ontario.

A pilot study of volunteers was conducted. These people had no known exposure patterns to Sr that might have led either to excess or deficiency of the element. Measurements were made at two sites, finger and ankle. Sr was clearly detectable in all 22 subjects who participated in the study⁴⁵⁾. There was a strong correlation between finger Sr and ankle Sr in these subjects, which confirmed that the method can distinguish with confidence between different levels of Sr in different subjects and that Sr levels were similar in these two different bones, supporting those literature reports that claim that Sr is approximately uniformly distributed in the different bones in the body⁴⁷⁾. In this pilot study, subjects of east Asian origin had significantly higher Sr levels than Caucasians. The difference was by a factor of between 2.5 and 3.0. Later a measurement was made of a Caucasian female who was taken a Sr salt in an attempt to strengthen her bones. She had a bone Sr level that was much higher than even the east Asian subjects, by a factor of between 5 and 10.

IV. Neutron Activation

There are two broad categories of neutron activation. In one the gamma-rays that are emitted promptly following neutron absorption are used as the measure of the element. Cadmium is the best example of an element that can be measured *in vivo* by this prompt gamma technique. In the alternative, neutron absorption (or some other neutron induced reaction) forms a product that is radioactive and it is emissions associated with the decay of this radioactive isotope that form the basis of the elemental measurement. Manganese and aluminium are examples of elements that can be measured in this way.

1. Cadmium in Liver and Kidney

It is possible to measure Cd in quite small quantities *in vivo* because one of the naturally occurring isotopes, ^{113}Cd has the extremely large cross section for capture of thermal neutrons of 20,000barn. ^{113}Cd is 12.26% abundant, so this yields an effective elemental cross section of about 2,500 barn. The product of the neutron capture, ^{114}Cd is stable, so it is the prompt gamma-rays that must be measured. This means that the irradiation and detection have to take place at the same time, which imposes constraints on system design in order to preserve reasonable detector performance. The original Cd measurement system was developed at the University of Birmingham Nuffield cyclotron using the $^9\text{Be}(^3\text{He},n)^{11}\text{C}$ reaction as a source of neutrons⁴⁸⁾. The ^3He beam was pulsed and so was the resultant neutron beam. This meant that gamma-ray counting took place in anticoincidence with a $20\mu\text{s}$ beam pulse. This significantly reduced background, particularly that arising from fast neutron events, rather than the thermal neutron events that

gave rise to the cadmium reaction. However, the greatest need for measuring Cd was in the context of occupational exposure and it became clear that it would be much more effective to take a Cd measuring device to the place of work, instead of relying on the workers to come to the cyclotron. So, a second generation system was devised, which used $^{238}\text{Pu/Be}$ neutron sources⁴⁹⁾ and it is a later version of this system which is now in place at McMaster⁵⁰⁾.

Two $^{238}\text{Pu/Be}$ sources, with a combined activity of 17Ci (0.63 TBq) are situated in a collimation and shielding assembly. The collimation is provided by an iron cylinder, set into a graphite block. This is then surrounded by alternating layers of high density polyethylene and iron. The neutron beam emerges from the central iron cylinder. The sample is placed in the neutron beam and hyperpure germanium detectors are placed to one side, offset from the direct neutron beam. Specific gamma-ray shielding is inset into the collimation box to reduce the fluence incident on the detectors from events in the box. The gamma-ray shielding comprises Pb, Hg, W (as heavy metal alloy) and Bi. Digital spectroscopy electronics and personal computer based multichannel analysers are used to process and record the signals from the detectors. The most prominent gamma-ray from Cd is at 559keV, from the first excited state of ^{114}Cd . This is used for the quantification of Cd.

In vivo Cd measurement systems, based on the neutron capture reaction were developed at several laboratories. Those that were most extensively used were at Birmingham and at the Brookhaven National Laboratory in the U.S.A. Although many studies were undertaken, those that had the greatest impact identified critical levels of Cd in the kidney⁵¹⁾, the corresponding levels in liver and the cumulative Cd in air exposures that would result in these critical levels being reached. The results from entirely independent studies at Brookhaven⁵²⁾ and at Birmingham⁵³⁾ agreed very closely. Kidney dysfunction, as evidenced by increased urinary excretion of low molecular weight proteins, for 50% of an exposed group was associated with a cumulative Cd in air figure of $1,000\mu\text{gCd.y/m}^3$ air. So, for example, a Cd in air concentration of $20\mu\text{gCd/m}^3$ air maintained for a 50 year working lifetime (with 40 hour working weeks) would give rise to the figure of $1,000\mu\text{gCd.y/m}^3$ air. $500\mu\text{gCd.y/m}^3$ air would result in 5% of a group exhibiting kidney dysfunction. At the time, regulatory levels were as high as $200\mu\text{gCd./m}^3$ air in at least one jurisdiction. The studies referred to here formed an important part of the evidence that resulted in revision of regulatory levels to a figure of $5\mu\text{gCd./m}^3$ air.

2. Manganese and Aluminium

There are considerable similarities between the measurement of manganese (Mn) and that of aluminium (Al). Both make use of a thermal neutron capture reaction, $^{55}\text{Mn}(n,\gamma)^{56}\text{Mn}$ for manganese⁵⁴⁾ and $^{27}\text{Al}(n,\gamma)^{28}\text{Al}$ for aluminium⁵⁵⁾. In both cases there is a direct interference from another element present in the body in a higher concentration, $^{56}\text{Fe}(n,p)^{56}\text{Mn}$ for manganese, $^{31}\text{P}(n,\alpha)^{28}\text{Al}$ for aluminium.

However, the neutron energy thresholds for the fast neutron reactions are 4MeV and 2MeV respectively. This means that an accelerator based neutron source can eliminate the possibility of these interferences. The ${}^7\text{Li}(p,n){}^7\text{Be}$ reaction is used, which has a laboratory frame proton energy threshold of 1.88MeV. Proton energies of between 1.9MeV and 2.25MeV are used, yielding maximum neutron energies of 0.55MeV. A neutron moderating and shielding assembly is used⁵⁶. This helps to ensure that the ratio of thermal neutrons to total equivalent dose is as high as it can be. It also minimises the radiation dose to all parts of a person's body other than that at which the measurement is being made. The shielding also ensures that accelerator operators and those conducting the measurement do not receive a significant radiation dose. Following irradiation, the subject moves to the counting area, where the induced activity is counted in a 4B NaI(Tl) counter⁵⁷. This comprises an assembly of 8 detectors, each of dimensions 102mm x 102mm x 408mm.

The half life of ${}^{56}\text{Mn}$ is 2.6h, so shorter lived activity, for example from ${}^{49}\text{Ca}$, is allowed to decay before the 847keV gamma-ray emitted following the decay of ${}^{56}\text{Mn}$ is counted for 30 minutes, starting an hour after the end of the neutron irradiation.

The half life of ${}^{28}\text{Al}$ is 2.3m and a gamma-ray of energy 1.78MeV is emitted following the decay. So, the count is started as soon as possible after the end of the irradiation and the duration of the count is about 5 minutes.

Manganese is an essential element; however, it can also be toxic in excess. Prolonged high level to respirable Mn has been associated with a movement disorder somewhat like Parkinson's disease⁵⁸. Lower levels of exposure have been associated with some loss of the ability to perform neurocognitive tasks. A pilot study is under way to determine whether Mn accumulates to a measurable extent in the bones of the hand in a group of welders, exposed occupationally to Mn, compared to the levels in a group of referent subjects.

Aluminium is not known to fulfill any vital role in human metabolism at the levels commonly encountered in contemporary environments. Excessive accumulation of Al does impair normal bone growth⁵⁹. There is also a continuing debate as to whether Al plays some role in the etiology of Alzheimer's disease⁶⁰. Earlier studies, particularly those at Brookhaven National Laboratory using their medical reactor demonstrated that Al could be measured in the bones of the hand and that the technique could be used to distinguish between the levels in long term dialysis patients and referent subjects⁶¹. The accelerator based system at McMaster is expected to have a somewhat lower detection limit than that at Brookhaven⁶². This system is in final trials prior to seeking ethical approval for an initial pilot study.

V. Conclusions

These Occupational Nuclear Medicine techniques provide information that is valuable and that could not be obtained in another way, with the possible exception of biopsy, which

carries quite strong disadvantages. The radiation doses required are low. A typical value for neutron activation of Mn is a maximum skin dose of 20mSv and an effective dose of the order of 20: Sv. For a prompt gamma Cd measurement the effective dose is similar, probably 40: Sv. The radiation doses required for *in vivo* x-ray fluorescence are even lower, being typically less than 0.1: Sv⁵.

Accepting these very positive aspects, it still should be emphasized that the Occupational Nuclear Medicine measurement does not normally supply all the information that is required to assess a person's situation. Rather the measurement should be used to complement information obtained by other measurements and observations.

Finally, the successful implementation of these techniques does require competence in radiation physics or a similar academic background. However, it is equally important that there is a collaborative team, including medical and health science researchers who ensure that relevant and important questions are posed for these techniques to answer.

Acknowledgement

The work at McMaster has received consistent support from the Natural Sciences and Engineering Research Council of Canada, through the Discovery grants program and through the Research Tools and Instruments program. Major equipment has been made available to this research through infrastructure awards made by the Canada Foundation for Innovation and the Ontario Innovation Trust.

References

- 1) J. Anderson, S.B. Osborn, R.W.S. Tomlinson, D. Newton, J. Rundo, L. Salmon, J.W. Smith, "Neutron activation analysis in man *in vivo*", *Lancet* ii, 1201-1205 (1964).
- 2) P. Chilibeck, A. Calder, D.G. Sale, C. Webber, "Reproducibility of dual-energy x-ray absorptiometry", *Canadian Association of Radiologists Journal*, 45, 297-302, (1994).
- 3) J.M. O'Meara, B.W. Blackburn, D.W. Chichester, D.P. Gierga, J.C. Yanch, "The feasibility of accelerator-based neutron activation analysis of nitrogen", *Applied Radiation and Isotopes*, 55, 767-774, (2001).
- 4) International Commission on Radiological Protection, Publication 23, Report of the task group on reference man, Pergamon, Oxford, (1975).
- 5) A.C. Todd, F.E. McNeill, J.E. Palethorpe, D.E. Peach, D.R. Chettle, M.J. Tobin, S.J. Strosko, J.C. Rosen, "*In vivo* XRF of lead in bone using K x-ray excitation with ${}^{109}\text{Cd}$ sources: radiation dosimetry studies", *Environmental Research* 57, 117-132, (1992).
- 6) L. Ahlgren, S. Mattsson, "Cadmium in man measured *in vivo* by x-ray fluorescence analysis" *Physics in Medicine and Biology*, 26, 19-26, (1981).
- 7) J. Börjesson, M. Isaksson, S. Mattsson, "X-ray fluorescence analysis in medical sciences: a review" *Acta Diabetologica*, 40, S39-S44, (2003).
- 8) S. Mattsson, B.J. Thomas, "Development of methods for body composition studies", *Physics in Medicine and Biology*, 51, R203-R228, (2005).
- 9) D.A. Bradley, M.J. Farquharson, "X-ray fluorescence and the *in vivo* evaluation of Fe, Cu, and Zn in skin", *Journal of*

- Radioanalytical and Nuclear Chemistry, 244, 213-217, (2000).
- 10) J.M. O'Meara, D.R. Chettle, F.E. McNeill, C.E. Webber, "The feasibility of measuring bone uranium concentrations in vivo using source excited K x-ray fluorescence" *Physics in Medicine and Biology*, 42, 1109-1120, (1997).
 - 11) R.C.N. Studinski, F.E. McNeill, D.R. Chettle, J.M. O'Meara, "Estimation of a method detection limit for an in vivo XRF arsenic detection system" *Physics in Medicine and Biology*, 50, 521-530, (2005).
 - 12) S.A. Graham, J.M. O'Meara, "The feasibility of measuring silver concentrations in vivo with x-ray fluorescence", *Physics in Medicine and Biology*, 49, N259-N266, (2004).
 - 13) J.O. Christofferson, S. Mattsson, "Polarised x-rays in xrf-analysis for improved in vivo detectability of cadmium in man", *Physics in Medicine and Biology*, 28, 1135-1144, (1983).
 - 14) R. Jonson, S. Mattsson, B. Unsgaard, "A method for in vivo analysis of platinum after chemotherapy with cisplatin", *Physics in Medicine and Biology*, 33, 847-857, (1988).
 - 15) J. Shakeshaft, S.C. Lillcrap, "An x-ray fluorescence system for the determination of gold in vivo following chrysotherapy", *British Journal of Radiology*, 66, 714-717, (1993).
 - 16) J. Börjesson, L. Barregard, G. Sallsten, A. Schutz, R. Jonson, M. Alpsten, S. Mattsson, "In vivo xrf analysis of mercury – the relation between concentrations in the kidney and the urine", *Physics in Medicine and Biology* 40, 413-426, (1995).
 - 17) L. Ahlgren, K. Lidén, S. Mattsson, S. Tejning, "X-ray fluorescence analysis of lead in human skeleton in vivo", *Scandinavian Journal of Work, Environment and Health*, 2, 82-86, (1976).
 - 18) L. Wielopolski, J.F. Rosen, D.N. Slatkin, D. Vartsky, K.J. Ellis, S.H. Cohn, "Feasibility of non-invasive analysis of lead in the human tibia by soft x-ray fluorescence", *Medical Physics* 10, 248-251, (1983).
 - 19) L. Wielopolski, J.F. Rosen, D.N. Slatkin, R. Zhang, J.A. Kalef-Ezra, J.C. Rothman, M. Maryanski, S.T. Jenks, "In vivo measurement of cortical bone lead using polarized x-rays", *Medical Physics* 16, 521-528, (1989).
 - 20) E.E. Laird, D.R. Chettle, M.C. Scott, "The factors affecting in vivo x-ray fluorescence of lead in bone", *Nuclear Instruments and Methods* 193, 377-382, (1982).
 - 21) L.J. Somervaille, D.R. Chettle, M.C. Scott, "In vivo measurement of lead in bone using x-ray fluorescence", *Physics in Medicine and Biology* 30, 929-943, (1985).
 - 22) L.J. Somervaille, "In-vivo measurement of tibia lead levels by x-ray fluorescence" PhD thesis, University of Birmingham, UK, 1984.
 - 23) C.L. Gordon, D.R. Chettle, C.E. Webber, "An improved instrument for the in vivo detection of bone lead", *British Journal of Industrial Medicine*, 50, 637-641, (1993).
 - 24) H. Nie, D.R. Chettle, L. Luo, J.M. O'Meara, "In-vivo investigation of a new ¹⁰⁹Cd g-ray induced K-XRF bone lead measurement system", *Physics in Medicine and Biology* 51, 351-350, (2006).
 - 25) D.E.B. Fleming, C.E. Mills, "A 4 x 500 mm(2) clover leaf detector system for in vivo bone lead measurement", *Medical Physics* 34, 945-951, (2007).
 - 26) S. N. Bateman, A. Pejović-Milić, I.M. Stronach, F.E. McNeill, D.R. Chettle, "Performance appraisals of digital spectroscopy systems for the measurement of bone lead" *Applied Radiation and Isotopes* 53, 647-650, (2000).
 - 27) L.J. Somervaille, D.R. Chettle, M.C. Scott, D.R. Tennant, M.J. McKiernan, A. Skilbeck, W.N. Trethowan, "In vivo tibia lead measurements as an index of cumulative exposure in occupationally exposed subjects", *British Journal of Industrial Medicine* 45, 174-181, (1988).
 - 28) J.O. Christofferson, A. Schutz, L. Ahlgren, B. Haeger-Aronsen, S. Mattsson, S. Skerfving, "American Journal of Industrial Medicine 6, 447-457, (1984).
 - 29) L. Gerhardsson, R. Attewell, D.R. Chettle, V. Englyst, N-G. Lundström, G.F. Nordberg, H. Nyhlin, M.C. Scott, A.C. Todd, "In vivo measurements of lead in bone in long-term exposed lead smelter workers", *Archives of Environmental Health*, 48, 147-156, (1993).
 - 30) J. Erkkilä, R. Armstrong, V. Riihimäki, D.R. Chettle, A. Paakkari, M. Scott, L. Somervaille, J. Starck, B. Kock, A. Aitio, "In vivo measurements of lead in bone at four anatomical sites: long term occupational and consequent endogenous exposure.", *British Journal of Industrial Medicine* 49, 631-644, (1992).
 - 31) J.A.A. Brito, D.E.B. Fleming, D.R. Chettle, "Structural analysis of relationships amongst bone lead, cumulative blood lead and current blood lead" *Proceedings of the European Conference on Energy Dispersive X-Ray Spectrometry*, 1998, ed.s J.E Fernandez, A. Tartari, 235-239, (1999).
 - 32) J.A.A. Brito, F.E. McNeill, C.E. Webber, D.R. Chettle, "Grid search: an innovative method for the estimation of the rates of lead exchange between body compartments" *Journal of Environmental Monitoring* 7, 241-247, (2005).
 - 33) J.A.A. Brito, F.E. McNeill, I. Stronach, C.E. Webber, S. Wells, N. Richard, D.R. Chettle, "Longitudinal changes in bone lead concentration: implications for modelling of human bone lead metabolism" *Journal of Environmental Monitoring*, 3, 343-351, (2001).
 - 34) H. Hu, "Bone lead as a new biologic marker of lead dose: recent findings and implications for public health", *Environmental Health Perspectives*, 106, 961-967, Suppl. 4 (1998).
 - 35) S.W. Tsaih, S. Korrick, J. Schwartz, C. Amarasiwardena, A. Aro, D. Sparrow, H. Hu, "Lead, diabetes, hypertension and renal function: the normative aging study", *Environmental Health Perspectives*, 112, 1178-1182, (2004).
 - 36) B.S. Glenn, K. Bandeen-Roche, B.K. Lee, V.M. Weaver, A.C. Todd, B.S. Schwartz, "Changes in systolic blood pressure associated with lead in blood and bone", *Epidemiology*, 17, 538-544, (2006).
 - 37) V.M. Weaver, B.S. Lee, A.C. Todd, K.D. Ahn, W.P. Shi, B.G. Jaar, K.T. Kelsey, M.E. Lustberg, E.K. Silbergeld, P.J. Parsons, J.Y. Wen, B.S. Schwartz, "Effect modification by delta-aminolevulinic acid dehydratase, vitamin D receptor, and nitric oxide synthase gene polymorphisms on associations between patella lead and renal function in lead workers", *Environmental Research* 102, 61-69, (2006).
 - 38) K. Chou, H. Hu, A. Ettinger, M. Tellez-Rojo, J. Schwartz, M. Hernandez-Avila, R. Wright, *Epidemiology* 17, S343, Suppl. S, (2006).
 - 39) T. Gonzalez-Cossio, K.E. Peterson, L.H. Sanin, E. Fishbein, E. Palazuelos, A. Aro, M. Hernandez-Avila, H. Hu, "Decrease in birth weight in relation to maternal bone-lead burden" *Pediatrics*, 100, 856-862, (1997).
 - 40) M. Hernandez-Avila, K.E. Peterson, T. Gonzalez-Cossio, L.H. Sanin, A. Aro, L. Schnaas, H. Hu, "Effect of maternal bone lead on length and head circumference of newborns and 1-month-old infants" *Archives of Environmental Health* 57, 482-488, (2002).
 - 41) P.J. Marie, M.T. Garba, M. Hott, L. Miravet, "Effect of low-

- doses of stable strontium on bone metabolism in rats”, *Mineral and Electrolyte Metabolism*, 11, 5-13, (1985).
- 42) W.E. Cabrera, I. Schrooten, M.E. De Broe, P.C. D'Haese, “Strontium and bone”, *Journal of Bone and Mineral Research*, 14, 661-668, (1999).
 - 43) R.E. Snyder, D.C. Secord, “The in situ measurement of strontium content in bone using x-ray fluorescence analysis”, *Physics in Medicine and Biology*, 27, 515-529, (1982).
 - 44) L. Wielopolski, D. Vartsky, S. Yasumura, S.H. Cohn, Application of xrf to measure strontium in human bone in vivo”, *Advances in X-Ray Analysis*, 26, 415-421, (1983).
 - 45) M. Zamburlini, A. Pejović-Milić, D.R. Chettle, C. Webber, J. Gyorffy, “In vivo study of an x-ray fluorescence system to detect bone strontium non-invasively” *Physics in Medicine and Biology* 52, 2107-2122, (2007).
 - 46) A. Pejović-Milić, J.A. Brito, J. Gyorffy, D.R. Chettle, “Ultrasound measurements of overlying soft tissue thickness at four skeletal sites suitable for in vivo x-ray fluorescence” *Medical Physics*, 29, 2687-2691, (2002).
 - 47) D.L. Thurber, J.L. Kulp, H.C. Hodge, P.W. Gast, J.M. Wampler, “Common strontium content of the human skeleton”, *Science*, 128, 256-257, (1958).
 - 48) J.S. McLellan, B.J. Thomas, T.C. Harvey, J.H. Fremlin, “Cadmium: its in vivo detection in man”, *Physics in Medicine and Biology*, 20, 88-95, (1975).
 - 49) B.J. Thomas, T.C. Harvey, D.R. Chettle, J.S. McLellan, J.H. Fremlin, “Transportable system for the measurement of liver cadmium in vivo”, *Physics in Medicine and Biology*, 24, 432-437, (1979).
 - 50) J. Grinyer, S.H. Byun, D.R. Chettle, “In Vivo Prompt Gamma Neutron Activation Analysis of Cadmium in the Kidney and Liver”, *Applied Radiation and Isotopes* 63, 475-479, (2005).
 - 51) H.A. Roels, R.R. Lauwerys, J.P. Buchet, A. Bernard, D.R. Chettle, T.C. Harvey, I.K. Al-Haddad, "In vivo measurement of liver and kidney cadmium in workers exposed to the metal. Its significance with respect to cadmium in blood and urine", *Environmental Research* 26, 217-240, (1981).
 - 52) K.J. Ellis, K. Yuen, S. Yasumura, S.H. Cohn, “Dose-response analysis of cadmium in man – body burden vs kidney dysfunction”, *Environmental Research* 33, 216-226, (1984).
 - 53) H.J. Mason, A.G. Davison, A.L. Wright, P.M. Fayers, K.M. Venables, N.J. Smith, C.J.G. Guthrie, D.R. Chettle, D.M. Franklin, M.C. Scott, H. Holden, D. Gompertz, A.J. Newman-Taylor, "A study of the relationships between liver cadmium, cumulative exposure and renal function in cadmium alloy workers", *British Journal of Industrial Medicine* 45, 793-802, (1988).
 - 54) M.L. Arnold, F.E. McNeill, I.M. Stronach, A. Pejovic-Milic, D.R. Chettle, A. Waker, “An accelerator based system for in vivo neutron activation analysis measurements of manganese in human hands” *Medical Physics*, 29, 2718-2724, (2002).
 - 55) A. Pejović-Milić, F.E. McNeill, W.V. Prestwich, A.J. Waker, D.R. Chettle, "Development of an accelerator based determination of aluminum burden in peripheral bone by neutron activation analysis." *Applied Radiation and Isotopes*, 49, 717-720, (1998).
 - 56) A. Pejović-Milić, S.H. Byun, D.R. Chettle, F.E. McNeill, W.V. Prestwich, “Development of an irradiation/shielding cavity for in vivo neutron activation analysis of manganese in human bone” *Journal of Radioanalytical and Nuclear Chemistry* 269, 417-420, (2006).
 - 57) S.H. Byun, W.V. Prestwich, K. Chin, F.E. McNeill, D.R. Chettle, “ 4π NaI(Tl) detector array for in vivo neutron activation analysis, *IEEE Transactions in Nuclear Science*, 53, 2944-2947, (2006).
 - 58) D.G. Ellingsen, L. Dubeikovskaya, K. Dahl, M. Chashchin, V. Chashchin, E. Zibarev, Y Thomassen, “Air exposure assessment and biological monitoring of manganese and other major welding fume components in welders”, *Journal of Environmental Monitoring*, 8, 1078-1086, (2006).
 - 59) H.H. Malluche, “Aluminium and bone disease in chronic renal failure”, *Nephrology Dialysis Transplantation*, 17, Suppl. 2, 21-24, (2002).
 - 60) J. Savory, C. Exley, W.F. Forbes, Y. Huang, J.G. Joshi, T. Kruck, D.R. McLachlan, I. Wakayama, “Can the controversy of the role of aluminum in Alzheimer's disease be resolved? What are the suggested approaches to this controversy and methodological issues to be considered?” *Journal of Toxicology and Environmental Health*, 48, 615-635, (1996).
 - 61) K.J. Ellis, S.P. Kelleher, “In vivo bone aluminum measurements in patients with renal disease”, in K.J. Ellis, S. Yasumura, W.D. Morgan (Eds.) *In Vivo Body Composition Studies*, Institute of Physical Sciences in Medicine, London, 464-468, (1987).
 - 62) A. Pejović-Milić, S.H. Byun, D.C. Comsa, F.E. McNeill, W.V. Prestwich, D.R. Chettle, In vivo measurement of bone aluminium: recent developments, *Journal of Inorganic Biochemistry* 99, 1899-1903, (2005).
-

Strategy for High Level Waste Management in China

CONG Huiling*

China National Nuclear Corporation, Beijing 100822, China

Geological disposal after reprocessing, conditioning and long-term storage is the framework of high level waste (HLW) policy adopted in China. Uranium and plutonium extracted from the spent fuels could be recycled. The HLW shall be disposed of in a centralized national deep geological repository. R&D on HLW disposal started in 1985 and some progress has been made on site selection and site characterization, buffer/back-fill material study, radionuclide migration study and safety assessment, etc.

KEYWORDS: nuclear power, spent fuel, high level radioactive waste, geological disposal

I. Nuclear Energy Development in China¹

The nuclear power program in China began in early 1980s and as of today the installed capacity is 8.7GWe (Table 1), which accounts for about 1.3% of the total installed capacity of electric power in China while the installed capacity for coal-fired power accounts for about 77% at the end of 2006. The massive coal burning causes environmental problems, mainly the urban air pollution.

Table 1 Nuclear power plants (NPPs) in operation in China^(a)

Nuclear plant ^(b)	Reactor type	Rated power MWe	1 st putting into grid	Distance to city
QSI	PWR	300	1991.12	90km to Hangzhou 120km to Shanghai
D Y B	1# PWR	900	1993.8	45km to Shenzhen, 50km to H.K.
	2# PWR	900	1994.2	
Q SII	1# PWR	600	2002.2	
	2# PWR	600	2004.3	
L A	1# PWR	1000	2002.2	
	2# PWR	1000	2002.12	
Q SIII	1# HWR	700	2002.11	
	2# HWR	700	2003.6	
T W	1# PWR	1000	2006.5	28km to Lianyungang
	2# PWR	1000	2007.5	

(a) NPPs in Taiwan province are not included.

(b) DYB: Da Ya Bay; QS: Qin Shan; LA: Lin Ao; TW: Tian Wan

Nuclear energy offers many advantages. It is safe, helps to guarantee a secure electricity supply, avoids exhausting precious fossil-fuel reserves, and involves no carbon-dioxide emissions, etc. In order to ensure sustainable development of the China's energy resources in the 21st century, nuclear power should play certain role as a mature and clean energy resource that can, to some extent, take place of fossil fuel.

A nuclear power program for the years of 2006-2020 has been drawn up in order to improve the energy structure and environment. The goal for nuclear power in the year of 2020 is that the installed capacity of nuclear power will be 40GWe with another 18GWe under construction, which will account for approximately 4 percent of total installed capacity of electricity by then. Most of the nuclear power plants are located at the coast areas (Fig. 1) because of the economic development and energy resource distribution. In the eastern region of China, which is economically developed but deficient in energy resources, nuclear power is the right way to meet the electricity demands and, also, avoid a long distance transportation of large amount of coal.

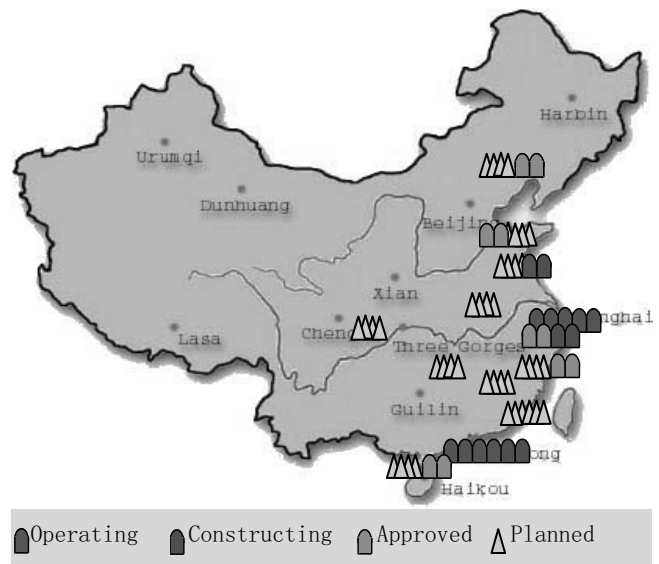


Fig. 1 NPP site distribution

On the road of active development of the nuclear power in China, safe management of radioactive wastes, especially the high level radioactive waste (HLW), has become a major challenge. HLW involves high radioactivity, chemical toxicity, significant heat release rate and very long life. Proper measures must be taken to isolate the HLW from the ecosystem to protect human health and the environment now and in the future from any unacceptable risk.

*Corresponding Author, Tel: +86-10-68555230, Fax: +86-10-68539146, E-mail: conghl@cnncc.com.cn

II. Radioactive Waste Disposal Policy

“The Law on Prevention and Control of Radioactive Contamination” was promulgated in 2003. It stipulates that the low and intermediate level radioactive waste shall be disposed of in the near surface repository regionally and the high level radioactive waste shall be disposed of in a centralized deep geological repository.

Regional near surface disposal has been implemented for years. The primary phase of the Northwest repository located near the Gobi desert has been put into operation. According to the plan, the repository with a total capacity of 200 thousand cubic meters will be completed by stages. For Phase I, the design capacity is about 60 thousand cubic meters in 18 disposal units, while that of the primary phase is about 20 thousand cubic meters in 6 disposal units. The Beilong repository in Guangdong province is about 5km away from the DYB nuclear power plant. The designed capacity of Phase I is 80 thousand cubic meters, and a capacity of 8800m³ for the primary phase has been completed.

The low and intermediate wastes shall be kept in the repositories for 300 years or more, and decay to a safe level.

We are in the process of research and development (R&D) for the deep geological disposal of HLW.

III. Strategy for HLW management

With the nuclear power development, the accumulated spent fuel will increase rapidly. The activity of radioactive waste produced during the nuclear fuel cycle exists mostly in the spent fuel, while the volume of mine tailings is the maximum as shown in **Table 2**. A typical composition of the PWR spent fuel with burn-up of 33GWd/tU is illustrated in **Table 3**. In long-term, the remaining radioactivity is mainly from trans-uranium nuclides with very long half-life, such as ²³⁷Np whose half-life is 2.14×10⁶ years. The β and γ radioactivities are mainly from fission products. ⁹⁰Sr and ¹³⁷Cs have the half-life of about 30 years but a few nuclides have very long half-life e.g. ⁹⁹Tc (2.13×10⁵ a), ¹²⁹I (1.57×10⁷ a) and ¹³⁵Cs (2.30×10⁶ a).

Table 2 Radioactive waste produced in the life of 1GWe PWR(33GWd/tU) Unit¹⁾

Waste	Volume (m ³)	Activity (Ci) (before decay)
Mine tailings	4.4×10 ⁶	3.7×10 ⁴
Once through cycle		
Uranium conversion	3.4×10 ²	9.8×10 ³
Uranium enrichment	1.3×10 ²	9.7×10 ³
Fuel element fabrication	3.1×10 ³	7.3×10 ⁰
Reactor operation	3.0×10 ⁴	2.9×10 ⁴
Spent fuel	5.2×10 ²	3.3×10 ⁹
		(a year after unloading)
Decommissioning		
LLW	1.5×10 ⁴	1.1×10 ⁵
Geological disposal	1.1×10 ²	4.1×10 ⁶
Total	4.4×10 ⁶	3.3×10 ⁹

The spent fuel shall be reprocessed according to the nuclear fuel cycle policy in China. The extracted uranium and plutonium could be recycled. High-level liquid waste thus generated, which contains minor actinides and fission products, will be vitrified and the glass forms or other conditioned HLW will be stored for years and then disposed of in a deep geological repository.

Table 3 A typical composition of the PWR spent fuel (33GWd/tU)¹⁾

Name	Weight (kg/tU)
Uranium	955
Plutonium	10
Actinides	1
Neptunium	0.4
Americium	0.3
Curium	0.03
Fission products	34
Structure material	300

The long term radioactive risks for different fuel cycles are shown in **Fig. 2**. Since the minor actinides and fission products are contained in the glass forms the radioactive hazards will last a very long time.

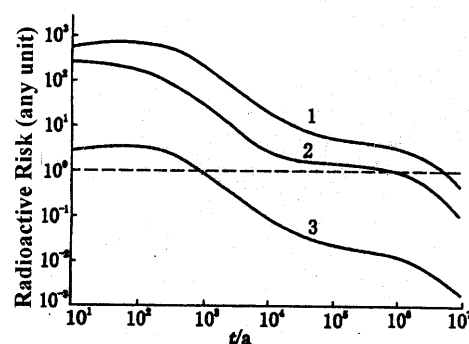


Fig. 2 Long term radioactive risks of different fuel cycles²⁾ (1 - Once through; 2 - 99.5% of U & Pu extracted by reprocessing; 3 - 99.5% of minor actinides extracted by reprocessing)

As a complementary measure, a research program on chemical partitioning of minor actinides and their transmutation in the fast neutron reactors has been put forward. A few very long half-life fission products may also be separated. Deep geological disposal, which isolates radionuclides from the environment, could thus benefit greatly from this reduction in toxicity of waste.

“Guideline for R&D Program of HLW Geological Disposal” has been issued in 2006 jointly by China Atomic Energy Authority, Ministry of Science and Technology and State Environment Protection Administration. The general goal of the R&D Program is to select a geologically stable site taking into consideration the social and economical conditions thereof, and to construct a national HLW repository in the middle of the century. It is by confinement and retardation of engineering barrier and geological barrier to protect the environment and public health from unacceptable harm of HLW.

Table 4 A preliminary working plan for the national HLW repository³⁾

Activities	Phase 1 (2001–2020)	Phase 2 (2020–2040)	Phase 3 (2040–2050)
		Site selection and site confirmation	URL construction and test
Site selection and characterization	Area/site selection, surface investigation, borehole drilling and test, complete site confirmation	Supplementary work for site characterization	Monitoring of the site
Underground research laboratory(URL)	Feasibility study, URL site recommendation, and design of URL	Construction of URL, test & demonstration of disposal technology	Part of test, monitoring of repository
HLW repository	Concept design	Preliminary design and detailed design	Construction completed around 2050
Research and development	Study on radionuclide migration, engineered barriers, performance assessment methodology	Studies on tests, radionuclide migration, engineered barriers, construction technology	Studies on repository closure, monitoring, etc.

The R&D and repository construction include three phases:

2006 - 2020 R&D in the laboratory and site selection;

2021 - 2040 Experiments and tests in the underground research laboratory (URL)

2041 to the middle of the century Verification, design and construction of a geological repository

The HLW disposal project will span more than a century from site selection to closure of the repository, during which many important decisions will be made. Because of unpredictable factors and the political sensitivity as well as the public acceptability, the work on the project has an exploratory nature in a certain sense and we have to make decisions step by step and pursue the project gradually and carefully.

Efforts must be made in following five aspects:

- (1) Enhancing decision-make management, a multi-discipline expert team organized as technical supports;
- (2) Establishing regulations and standards, defining the safety objective, environmental requirement, fund raising drives, regulatory procedure and relative technical requirements.
- (3) Optimizing resource allocation for scientific study;
- (4) Strengthening the communication with the public and local government;
- (5) Promoting international or bilateral cooperation.

R&D on HLW disposal was started in China in 1985. Some progress has been made with regard to site selection and site characterization, buffer/back-fill material study, radionuclide migration study and safety assessment etc. Nation-wide site screening, regional and sub-regional screening have been conducted. The Beishan area of Gansu province in northwest China has been considered as a potential site, where the surface geological, hydro-geological, geophysical survey and borehole drilling were carried out. Further site characterization will be performed, for which commitment of IAEA assistance has already been obtained through its technical cooperation project.

The buffer/back-fill material is one of the main engineered barriers for the repository. A comprehensive investigation shows that there are 84 main bentonite deposits in China. The study on bentonite properties, including the coupled thermo-hydro- mechanical process is under way.

The radionuclides in migration study include ²³⁹Pu, ²³⁷Np, ²⁴¹Am, ⁹⁹Tc, ¹³⁴Cs, ¹³⁷Cs, ⁹⁰Sr. The media studied include granite, bentonite, granite fractures and some metallic minerals.

A framework of safety assessment for HLW disposal shall include aspects of infrastructure; safety principles and safety objectives; safety requirements for engineering barrier systems and site performance assessment, and an integrated safety assessment.

A preliminary working plan for the national HLW repository has been proposed by some scientists in China. The plan envisions the following steps: first, the site characterization of the potential site (Beishan area) then the construction of a site-specific URL at the potential site for HLW repository and, finally, the construction of HLW repository(**Table 4**). However, consensus has yet to be reached on the plan.

The debate is mainly focused on host rock (granite or clay?); URL (site specific or general URL? when to set up?); the time frame for safety assessment; retrievability (long term storage or permanent?). The HLW geological disposal involves many technical areas such as geology, hydrogeology, chemistry, environmental safety etc. The waste forms contain several tens nuclides and possess very high activity, which will be affected by the thermal–hydro–stress–chemical coupled reaction under high temperature and high pressure as well as the seismic or geological structure movement etc. That makes the study very complicated and difficult. Some issues need to be studied, such as the uncertainty of the data and model in the deep geological environment, the credibility of time and space extrapolating, a methodology for deterministic and probabilistic safety assessment etc.

IV. Conclusion

Geological disposal after reprocessing, conditioning and long-term storage is the framework of HLW policy adopted in China. The deep geological repository is a complicated and systematic engineering project. The key is to confine and retard the radionuclides by multi barriers for purpose of protecting the environment and public. The main challenge is to implement management methods that are acceptable to the public, cost-effective, and environmentally friendly.

Great progress has been made in recent years on the safety management of the high level radioactive waste. However, we will still meet a lot of challenges in the coming years. We will make every effort to control the radioactive wastes effectively so as to ensure the sustainable development of the nuclear power.

References

- 1) Zhu Y J, Attention to Systematic Study on Nuclear Fuel Cycle and Nuclear Waste Disposal, Radiation Protection Forum, 2005
- 2) Gu Z M, Ye G A, Recent Developments in studies of Advanced Nuclear Fuel Cycle System, Atomic Energy Science and Technology 2002, 36: 160 – 167.
- 3) Wang J, Strategic program for deep geological disposal of high-level radioactive waste in China, Uranium Geology, 2004, 20: 196 - 204.
- 4) Chen S, Discussions on safety assessment for HLW disposal, Radiation Protection Bulletin, 2005, 1.

Radiation Dosimetry in Brachytherapy, Introducing A Spherical Diode Dosimeter

Gad SHANI^{1*}, Leon LIUBIMOV², Amal AYOUB¹, Andrei BROISMAN¹, and Irit LEVINGER¹

¹Department of Biomedical Engineering, Ben Gurion University, Beer Sheva, Israel

²Oncology Division, Sheba Medical Center, Israel

Brachytherapy is a cancer treatment modality in which a radiation source is inserted into the tumor. It is done in one of two ways: Low Dose Rate (LDR) treatment where seeds are permanently implanted, or High Dose Rate (HDR), a short time exposure. The isotopes mostly used for LDR treatment are I-125 and Pd-103 of activity about 18.5 MBq per seed. HDR treatment is generally done with Ir-192 sources of activity 370 GBq. We introduce a new source for both HDR and LDR treatment, namely Tm-170. Safety considerations for the medical staff, the patient and people around him include: well shielded sources, shortest handling time and keeping uninvolved people at a safe distance. HDR sources are kept in a lead container and applied by a remote controlled delivery system. Radiation dosimetry and source calibration is done before the sources are applied to the patient. The methods used for dose measurement are: TLD, diode or ion chamber. We introduced a new diode for dosimetry, micro-spherical diode. This tiny diode causes very little perturbation and provides spherically symmetrical dose measurements. Monte Carlo calculations are used to verify the measurements. Source parameters are calculated for source quality comparison.

KEYWORDS: brachytherapy, safety, dosimetry, spherical diode, thulium seeds

I. Introduction

Brachytherapy (short distance therapy) is a radiation therapy modality used to treat cancer. It is also called internal radiation therapy. It is done at either low dose rate or high dose rate.

Low dose rate (LDR) brachytherapy is achieved by placing radioactive seeds permanently into the tumor or its surrounding material. The most common radioactive isotopes used for low dose rate brachytherapy are I-125 and Pd-103. These deliver their dose at low rate and stay in the body till completely decayed.

High dose rate (HDR) is obtained by inserting high activity isotope generally Ir-192, of activity of 370 GBq for 10 minutes to a couple of hours. The source is then removed from the patient. The treatment might be repeated several times until the desired dose is obtained.

Brachytherapy is an out patient procedure. Seed implantation takes less than an hour. High dose rate treatment might be even shorter, so the patient leaves the hospital the day of the treatment. There is little discomfort after the implantation. The symptoms usually go away in a few day or a week.

Permanent seed implant alone (monotherapy) is used to treat prostate cancer which has high probability of being confined to the prostate. Dose can be controlled by changing the number of seeds, seeds activity, changing energy by changing radioisotope, period of irradiation and seed location. Different cancers respond to different radiation treatment.

Computerized Tomography imaging prior to seed implantation is used for determining the exact position of seed implantation. Ultrasound imaging is used for real time seed location.

Patients carrying implanted seeds in their body are not a radioactive risk to the general public. The dose emitted from such patient is of the order of 0.2 μ Sv/h.

One of the advantages of HDR over LDR Permanent seeds implantation is the ability to evaluate the implant in 3D before treatment is given. An example of a recent treatment planning image is shown in Fig. 1.

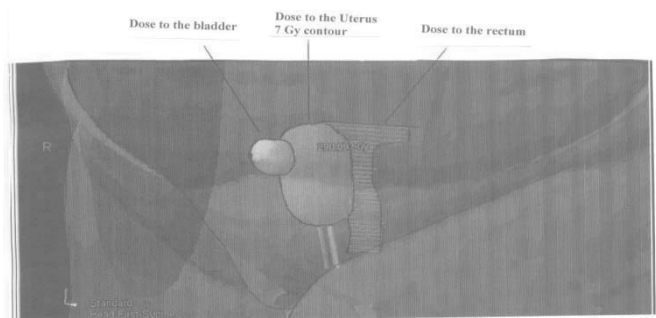


Fig. 1 Three dimensional computer imaging of dose to organs around the tumor. The main volume describes the 7.00 Gy dose limit. The dose to the bladder (small sphere to the left) is about 2.5 Gy and the dose to the rectum (area to the left) is about 1.5 Gy.

Dose volume histogram is plotted, telling the physician how much of the target volume is covered by the 100% prescription dose and how much of the dose to the rectum and bladder receive. The plot for the patient mentioned in Fig. 1 is shown in Fig. 2.

*Corresponding Author, Tel: 972 8 6479638, Fax: 972 8 6479632, E-mail: gshani@bgu.ac.il

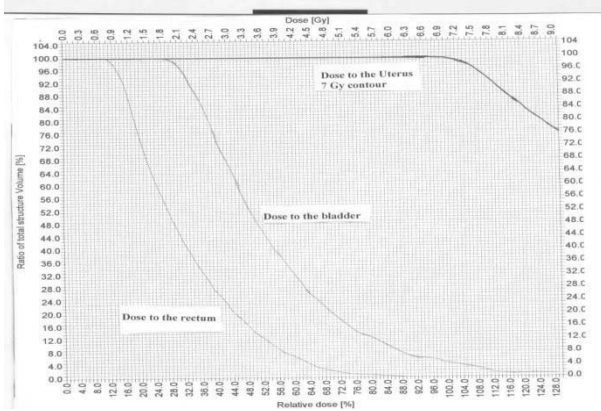


Fig. 2 Lines describing the dose and percent of organ volume exposed. 100% of the uterus is exposed to 7.00 Gy

Another problem with LDR is that after the implant the gland frequently swells. This swelling can displace the seeds increasing the distance between them, therefore create cold spots.

Some disagreement can be found in the literature regarding the preferred half life of seeds used for brachytherapy. It is better that the seed delivers all its dose within a short time, or, since some tumor are slow growing, therefore longer half life is better.¹⁾ The most common short half life seed used is Pd-103. I-125 on the other hand has a half life more than 3 times longer.

Pd-103 gives off its energy relatively fast ($T_{1/2}=17$ days). No clinical data suggests that fast is better. Because prostate cancer is generally a slow growing tumor, radiation from fast decaying sources might be wasted.

Because of the difference in half-lives it was suggested that I-125 ($T_{1/2}=60$ d) is used for slow growing tumors (low Gleason Score – rate of cells doubling time), and Pd-103 is used for fast growing tumors (high Gleason Score).²⁾ We have developed Tm-170 with half life of 128 days as a source for both LDR and HDR. Among other advantages of this seed it is ideal for slow growing tumors.³⁾

II. Dose Rate Parameters Calculation

Dosimetry methods of brachytherapy sources have been thoroughly investigated and developed during the last two decades. Standard parameters for each source became a standard of acceptance of the source for clinical use. Certain parameters must be measured and/or calculated.⁴⁾ The recommended protocol for dose calculation formalism is based on measured or calculated quantities. It allows calculation of two-dimensional dose distribution around the source. The dose rate at distance r from a source is calculated assuming a point source or a line source approximation. The latter is a more realistic situation, therefore a two dimensional source of length L is assumed. The dose rate is calculated assuming a cylindrical symmetric source. The dose rate $\dot{D}(r, \theta)$ at point (r, θ) is given by:

$$\dot{D}(r, \theta) = S_k \cdot \Lambda \cdot \frac{G(r, \theta)}{G(r_0, \theta_0)} \cdot F(r, \theta) \cdot g(r),$$

where S_k is air kerma strength or air kerma rate,

Λ is the dose rate constant, it is defined as the dose rate to water at a distance 1 cm on the transverse axis of a unit air kerma source in a water phantom.

$G_p(r, \theta)$ (or $G_L(r, \theta)$) is the geometry function for a point source or a line source,

$g_L(r)$ is the radial dose function, accounting for dose fall-off on the transverse plane due to photon scattering and attenuation, and

$F(r, \theta)$ is the anisotropy function.

This equation is well known and widely used among seed developers; we used it for calculating our Tm-170 seeds parameters.⁵⁾ Methods were developed for the calculation of each one of the parameters above.

The American Association of Physics in Medicine has defined the dose rate constant as the dose rate at 1 cm along the perpendicular bisector of the source divided by the air kerma strength of the source, U ($\text{cGy cm}^2 \text{h}^{-1}$). Consequently the units of the dose rate constant are cGy/h per U .⁶⁾

Monte Carlo calculations of dose to liquid water in liquid water medium yield a value of 0.92 cGy/h per U . When the medium is changed to solid water, the Monte Carlo calculations yield a dose rate constant of 0.88 cGy/h per U .⁷⁾ The composition of solid water does not exactly mimic that of liquid water at the photon energies obtained from an I-125 brachytherapy source. Therefore the effects of the phantom composition on the measurement of dose rate constant are usually calculated using Monte Carlo calculation.

The Monte Carlo simulation done by Ibbott⁶⁾ estimated the dose to selected materials as a function of the contained activity of the source. For these calculations the simulation is performed to determine the dose to air, in an air medium, it is effectively the air kerma. The results yielded a dose rate to air in air medium (or air kerma rate) of 0.726 cGy/h at a distance of 1cm along the perpendicular bisector of the source. The calculation assumed a contained source of 37 MBq. The air kerma rate is therefore $0.196 \text{ mGy cm}^2 \text{h}^{-1} \text{MBq}^{-1}$.

Relative dose as a function of distance for some sources is shown in **Fig. 3**.

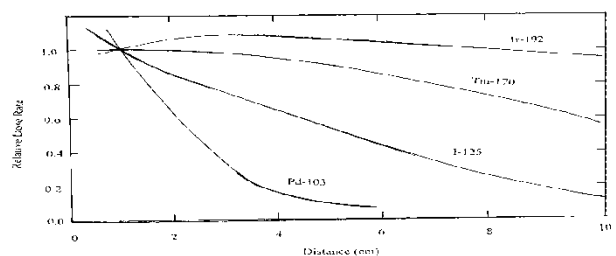


Fig. 3 Relative dose rate in tissue equivalent plastic as a function of distance from the source for various sources

III. Safety Measures

For low dose rate, a $7.6 \times 7.6 \text{ cm}^2$ template is attached to the ultrasound. This template has holes every 0.5 cm through which the needles are placed. The rectal ultrasound is moved until a nice image of the prostate is seen on the monitor.

Under ultrasound visualization a non-radioactive gold seed is injected into the lowest part of the prostate gland. This is served as a reference marker for the CT scan. Then the needles loaded with the seeds according to the treatment planning, are inserted using hollow plastic needles with a movable metal insert. The needles are 23.5 cm long, 2 mm diameter. These are placed through the template, through the skin and into the prostate gland. The number of needles is 12-32.

Mick applicator is used for seeds implantation. Loading the Mick applicator with seeds is done using a head and torso shield. This is a 9.5 mm thick aluminum shield of dimensions 28x30 cm and a lead glass window of dimensions 25x20 cm, 6.25 mm thick, equivalent of 0.56 mm lead. This is equal to 22 HVL (Half Value Layer) for I-125 seeds. For 100 I-125 seeds of activity 14.8 MBq, the exposure behind the lead glass is negligible.

For high dose rate, after the patient goes through CT imaging an image of the tumor is obtained. The physician makes the decision regarding the dose to the tumor and the volume surrounding it. Treatment planning is done by the medical physicists. This planning tells the implanting personnel the number of source, the location and the dwelling time of the sources in the tumor. Generally the physician instructions are the dose limit (minimum dose) delivered to a certain volume. The treatment planning is done with the aid of a computer program that provides isodose surfaces and volumes. The computer provides a three dimensional drawing of the doses at volumes as illustrated in **Fig.1**. In addition to the desired dose to the tumor, the treatment planning provides the dose to area where the dose must be low as shown in **Fig. 2**.

Seeds calibration, both for HDR and LDR is done in a well type ion chamber and a sensitive electrometer (0.001pA to 100nA or 0.37 mBq to 37 MBq). For HDR seeds, the calibration ion chamber is connected to the machine with plastic tubing as it is done to the patient for treatment, and the source is sent into the calibration detector by the remote control system. For LDR calibration, a seed or a number of seeds in a magazine or in seed in strand (seeds in plastic tubing with spacers between them), are inserted to the calibration system behind a shield.

Seeds are leak tested by the manufacturer before shipment for implantation. The activity rubbed off in a smear test should be smaller than 185 Bq. Unused seeds must be kept for 6 months before disposed of. Up to 120 seeds are implanted in the patient gland.

Loss of seeds from the patient's body can be detected in a CT imaging done a month after implantation. Patients containing permanent implants may be released from radiation isolation when the dose rate at 1m from the patient falls below 50 μ Sv/h.

IV. New Dosimeter – Microspherical Diode

Dosimetry for brachytherapy is generally done with TLD, planar diodes or ion chamber. Neither of those dosimeters provides spherically symmetric measurement of the dose,

since they have a preferred direction or a direction to which it is more sensitive. They also cause a serious perturbation of the dose distribution.

Since the source is located in the tumor and its radiation is emitted in all directions, scattered radiation comes back from all directions. Therefore in order to get the correct dose at any given point, the dosimeter should be equally sensitive to all directions. The dosimeter should also be of small dimensions to cause a minimal perturbation.



Fig. 4 The phantoms used for dosimetry in the present work, 10cm diameter by 10cm high and 20cm diameter by 20 cm high PMMA cylinders

We applied a micro-spherical diode made by Kyoto Semiconductor Corp. as a dosimeter. The diode has a diameter of 1.8 mm, inner core made of p type Si, covered by an n type Si spherical shell. The advantage of this diode, in addition to being a symmetrical detector, is its miniature size. The measurements were done in Perspex phantoms shown in **Fig. 4**. The dimensions are: 10 cm diameter by 10 cm high or 20 cm diameter by 20 cm high. The diode current as a function of distance between the diode and an I-125 seed does not show a $1/r^2$ falloff because of backscattering from the phantom's material. The most important measurement is the one that verifies the spherically symmetric sensitivity of the diode. It was done with the diode placed at a center of a circle and the I-125 seed placed at 12 different positions on the circle (every 30°). The results show that the diode sensitivity is perfectly spherically symmetrical, as shown in **Fig. 5**. Three different seeds were placed at a distance of 6 mm from the diode.⁸⁾

We have compared these measurements with those made with a planar diode, made by Detection Technology, model XRB, of sensitive area 5x5 mm. This diode "sees" radiation coming in an angle of 180 degrees to its sensitive surface. It was found that when the source is placed in front of the square diode, it is 10 times more sensitive than the spherical diode.

In addition, we have made Monte Carlo calculations. The fit between the measurements and the calculations was very good.

LiF(Mg,Ti) TLD measurements were used for diode calibration.

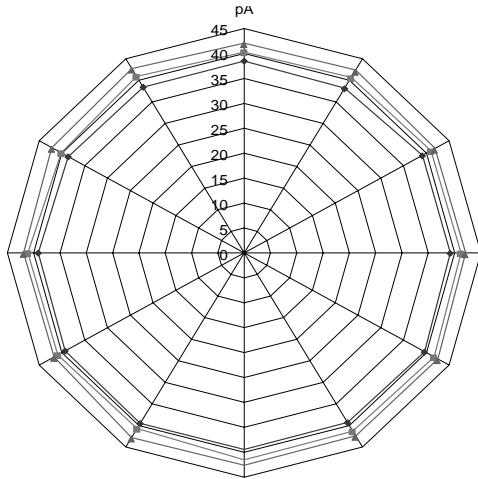


Fig. 5 2π dose measurement around the spherical diode dosimeter. Results for three different seeds are shown.

V. Tm-170 seeds dosimetry

Tm-170 seeds for brachytherapy were made by neutron activation of 4.46 mg of thulium ($0.2 \times 0.6 \times 4$ mm) inside titanium tubes of 0.8 mm outer diameter, 0.7 mm inner diameter, and 7 mm long. Tm-170 emits x-rays of the following energies: 7.42 keV (4%), 51.35 keV (1.2%), 52.39keV (2.2%) and 59.4 (0.9%), and gamma ray of energy 84.25 keV (3.25%). Tm-170 also emits beta rays of energies 883 keV (24%) and 968 keV (76%).⁹⁾

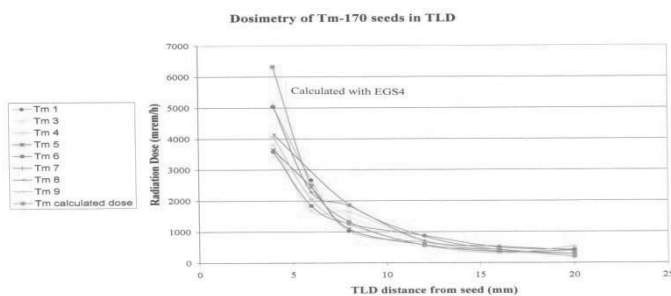


Fig. 6 The dose as a function of distance from Tm-170 seeds as measured with TLD100 and calculated with EGS4

Eight seeds were prepared as described. Dosimetry of these seeds was carried out in cylindrical Perspex phantom

with a hole at the center, where seeds could be placed. Six LiF (Mg, Ti) crystals with dimensions of $3.2 \times 3.2 \times 0.9$ mm were placed at different distances from the source, results are shown in **Fig. 6**. The results of TLD measurements are compared to EGS4 calculations. The different dose rates of the seeds is due to the fact that the activation flux was not perfectly uniform over the seeds package during activation. The measured dose rates are from exposure to gamma- and x-rays from Tm-170, beta rays are absorbed in the Perspex within the 3.5 mm diameter.

VI. Conclusions

Brachytherapy seems to be a safe cancer treatment modality. Radiation level is controled so that high dose is delivered to the tumor only, while sparing the neighboring organs. Source calibration is generally done using TLD measurements and Monte Carlo calculation methods. A new 4π dosimeter is proposed for brachytherapy namely a spherical diode. These diodes showed perfect 4π symetry of it's sensitivity. Being of small dimentions, their perturbation of dose distribution is very small.

In addition a new brachytherapy source namely Tm 170 is presented. It shows a very useful dose distribution and seems to be a very promising future source for brachytherapy.

References:

- 1) J.C. Blasko, P.D. Grimm, J.E. Sylvester, K.R. Badiozamani, D. Hoak, W. Cavanagh, Palladium-103 brachytherapy for prostate carcinoma. *Int J Radiat Oncol Biol Phys* 46(4), 839,(2000).
- 2) S. Marks, Prostate and Cancer, Fisher Books LLC, USA, (1999)
- 3) G. Shani, A. Hwaree, I. Orion, Development of new brachytherapy seeds based on Tm-170. 5th International Conference on Isotopes, p.29, Brussels, April (2005).
- 4) M. J. Rivard et al, Update of AAPM Task Group 43 Report: Protocol for brachytherapy dose calculations. *Med. Phys.* 31 (3), 633, (2004).
- 5) D. Silvern, A. Ayoub, G. Shani, Automated Generation of TG-43 Parameters for a Brachytherapy Source. IAEA – Ben Gurion University Workshop Nov. 7-8, 2007.
- 6) G.S. Ibbott, A.S. Meigooni, Determination of dose rate constant. University of Kentuky report, (1999).
- 7) G.S. Ibbott, Estimate of contained activity. University of Kentucky report, (1999).
- 8) G. Shani, A. Broisman, 4π Dosimetry for brachytherapy using micro-spherical diodes. World Congress on Medical Physics and Biomedical Engineering, Seoul, (2006)
- 9) A. Ayoub, Development of new radioactive seeds Tm-170 for brachytherapy combined with Auger electron emission. Ph. D. Thesis, Ben Gurion University, Beer Sheva Israel, (2007)